

INFORMATION TO USERS

This manuscript has been reproduced from the microfilm master. UMI films the text directly from the original or copy submitted. Thus, some thesis and dissertation copies are in typewriter face, while others may be from any type of computer printer.

The quality of this reproduction is dependent upon the quality of the copy submitted. Broken or indistinct print, colored or poor quality illustrations and photographs, print bleedthrough, substandard margins, and improper alignment can adversely affect reproduction.

In the unlikely event that the author did not send UMI a complete manuscript and there are missing pages, these will be noted. Also, if unauthorized copyright material had to be removed, a note will indicate the deletion.

Oversize materials (e.g., maps, drawings, charts) are reproduced by sectioning the original, beginning at the upper left-hand corner and continuing from left to right in equal sections with small overlaps.

Photographs included in the original manuscript have been reproduced xerographically in this copy. Higher quality 6" x 9" black and white photographic prints are available for any photographs or illustrations appearing in this copy for an additional charge. Contact UMI directly to order.

ProQuest Information and Learning
300 North Zeeb Road, Ann Arbor, MI 48106-1346 USA
800-521-0600

UMI[®]

University of Alberta

Mathematical models for vasomotion and the myogenic response

by

Christopher Meyer



A thesis submitted to the Faculty of Graduate Studies and Research in partial
fulfillment of the requirements for the degree of Master of Science in Applied
Mathematics

Department of Mathematical Sciences

Edmonton, Alberta

Fall 2000



National Library
of Canada

Acquisitions and
Bibliographic Services

395 Wellington Street
Ottawa ON K1A 0N4
Canada

Bibliothèque nationale
du Canada

Acquisitions et
services bibliographiques

395, rue Wellington
Ottawa ON K1A 0N4
Canada

Your file *Votre référence*

Our file *Notre référence*

The author has granted a non-exclusive licence allowing the National Library of Canada to reproduce, loan, distribute or sell copies of this thesis in microform, paper or electronic formats.

The author retains ownership of the copyright in this thesis. Neither the thesis nor substantial extracts from it may be printed or otherwise reproduced without the author's permission.

L'auteur a accordé une licence non exclusive permettant à la Bibliothèque nationale du Canada de reproduire, prêter, distribuer ou vendre des copies de cette thèse sous la forme de microfiche/film, de reproduction sur papier ou sur format électronique.

L'auteur conserve la propriété du droit d'auteur qui protège cette thèse. Ni la thèse ni des extraits substantiels de celle-ci ne doivent être imprimés ou autrement reproduits sans son autorisation.

0-612-59847-0

Canada

University of Alberta

Library Release Form

Name of Author: Christopher Meyer

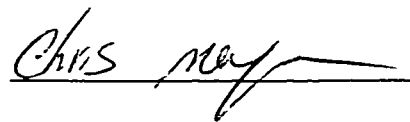
Title of Thesis: Mathematical models for vasomotion and the myogenic response

Degree: Master of Science

Year this Degree Granted: 2000

Permission is hereby granted to the University of Alberta to reproduce single copies of this thesis and to lend or sell such copies for private, scholarly or scientific research purposes only.

The author reserves all other publication and other rights in association with the copyright in the thesis, and except as herein before provided, neither the thesis nor any substantial portion thereof may be printed or otherwise reproduced in any material form whatever without the author's prior written permission.

A handwritten signature in cursive script, reading "Chris Meyer", written over a horizontal line.

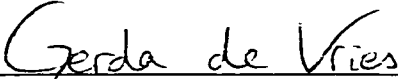
Christopher Meyer
32 Kristi Court,
Sudbury, Ontario, Canada
P3E 5R5

September 21, 2000


UNIVERSITY OF ALBERTA

Faculty of Graduate Studies and Research

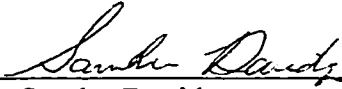
The undersigned certify that they have read, and recommend to the Faculty of Graduate Studies and Research for acceptance, a thesis entitled **Mathematical Models for Vasomotion and the Myogenic Response** submitted by **Christopher Meyer** in partial fulfillment of the requirements for the degree of **Master of Science** in Applied Mathematics.



Dr. Gerda de Vries (Supervisor)



Dr. James S. Muldowney (Chair)



Dr. Sandra Davidge
(Perinatal Research Centre, Depts of
Obstetrics/Gynaecology and Physiology)

Date:

Abstract

Small blood vessels are more than inert tubes that carry blood. They are elastic and surrounded by muscle that contract or relax to alter the local blood flow characteristics. The regulation of blood flow by the muscle is called the *myogenic response*. Blood vessels are also observed to exhibit *vasomotion*, which is the spontaneous oscillation of the vessel diameter.

In the first part of the thesis, a controversy in the published literature on the effect of vasomotion on vascular resistance is resolved. A mathematical model is used to show that vasomotion decreases the effective vascular resistance. In the last part of the thesis, a model describing the dynamics of vasomotion is reviewed and analyzed. In addition, the model is modified to include three theories on the mechanisms underlying the myogenic response. The model can qualitatively predict characteristics of the myogenic response, and serves as a good foundation for future models.

Acknowledgments

I wish to express my sincere appreciation and gratitude to the following individuals for their assistance.

To Dr. Gerda de Vries, my supervisor, for absolutely everything.

To Dr. Sandra Davidge, for sharing her expertise in physiology.

To Mr. John Savage, for introducing me to the wonders of mathematics.

To Renate and Wilfried Meyer, my parents, for their neverending support.

To Ania, for always listening to my ideas and challenging my mind with a good physics debate.

Thank you all.

Contents

1	Introduction	1
2	Effect of vasomotion on vascular resistance	6
2.1	Poiseuille's law	7
2.2	Background, setup, and analysis of the model	10
2.3	The use of Poiseuille's law in modeling the effect of vasomotion on vascular resistance	14
2.3.1	Argument 1 - Slow varying wall radius	15
2.3.2	Argument 2 - Stokes number	16
2.3.3	Argument 3 - Fast transient to a similar problem	18
2.4	Discussion	19
3	A mathematical model of smooth muscle activity	22
3.1	Model derivation	23
3.1.1	Smooth muscle mechanics	24
3.1.2	Muscle stress development and the dependence on in- tracellular calcium	30

3.1.3	Electrophysiology and intracellular calcium concentration of vascular smooth muscle	33
3.2	Model summary	37
3.3	Model analysis	39
3.4	Discussion	42
4	The myogenic response and the regulation of myogenic tone	43
4.1	Initiation of the myogenic response	47
4.1.1	Stretch-activated channels (SAC)	48
4.1.2	Intracellular calcium stores and IP ₃	52
4.2	A mechanism for the maintenance of myogenic tone	58
4.3	Discussion	59
5	Discussion and conclusions	62
	Bibliography	68

List of Tables

3.1	Model parameters and their default values	40
4.1	Parameters used in the modified model that incorporates the intracellular calcium stores	55

List of Figures

1.1	Experimental record of vasomotion observed in an artery of a pregnant rat	2
2.1	Normalized volume flux, resistance, and effective resistance as functions of vasomotion amplitude	12
3.1	Curves of elastic and muscle stress as functions of radius . . .	27
3.2	Free body diagram of forces assumed in the vessel wall	29
3.3	Overlapping thin and thick filaments of smooth muscle	31
3.4	Fraction of open calcium channels as a function of the membrane potential	36
3.5	Phase plane analysis of the vasomotion model	41
3.6	Solution of the vasomotion model as a function of time	41
4.1	The myogenic response in the skeletal muscle vascular bed of the dog	44
4.2	Steady-state solution of the model modified to include stretch-activated channels	46

4.3	Nullclines in the (v, r) phase plane for the model modified to account for stretch-activated channels	50
4.4	Steady-state dependence of the membrane potential and vessel radius on the fraction of open stretch-activated channels . . .	51
4.5	Experimental record of the relative change in intracellular IP_3 concentration of vascular smooth muscle after a single 20% stretch	53
4.6	Solution of the vasomotion model modified to account for IP_3 -induced release of calcium from the intracellular stores	57
4.7	Steady-state dependence of muscle activation and radius on the calcium concentration sensitivity parameter	60

Chapter 1

Introduction

The blood vessels that are primarily responsible for the regulation of blood flow through the body are called *resistance vessels* [1]. Resistance vessels are the precapillary vessels that regulate blood flow to the capillary beds [1]. For these vessels, the pulsatile pressure from the heart is negligible and the intraluminal pressure gradient is roughly constant. It is these vessels that are of interest in this thesis.

Resistance vessels can locally regulate blood flow by contracting or relaxing the thick layer of *smooth muscle* which surrounds the vessel. For example, the increase in blood flow resulting from an increase in blood pressure can be counteracted by muscle contraction. Muscle contraction reduces the vessel radius which returns blood flow to control levels. This mechanism of blood flow regulation is referred to as *autoregulation* or the *myogenic mechanism* [1].

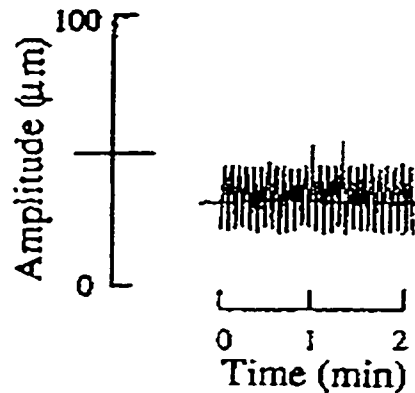


Figure 1.1: Strip-chart recording of an artery undergoing vasomotion from a pregnant rat. Figure taken from Gratton et al. [11].

Resistance vessels are also observed to exhibit *vasomotion* [17]. *Vasomotion* is the spontaneous rhythmic contraction and relaxation of the vascular smooth muscle which results in an oscillation of vessel radius. *Vasomotion* was first observed in bat wing veins in 1852, and was soon after observed in rabbit ear arteries and the frog web small arteries [12]. A typical experimental record of *vasomotion* is shown in Figure 1.1. The functional significance of *vasomotion* is not established, although there is little doubt that it has an effect on blood flow and *vascular resistance*. It has been proposed that *vasomotion* is related to the myogenic response [7, 32, 33], or that it results from an instability in the system that controls smooth muscle intracellular calcium levels [32].

The content of this thesis is divided into two parts. The first part, contained in Chapter 2, analyzes the effect of *vasomotion* on *vascular resistance*.

Vascular resistance is defined locally on a segment of blood vessel as [24]

$$R_V = \frac{\Delta p}{F}, \quad (1.1)$$

where Δp is the pressure drop over the length of the vessel (intraluminal pressure) and F is the fluid volume flux. The definition of vascular resistance is analogous to Ohm's law ($R = \frac{V}{I}$), which relates the resistance, voltage, and current in basic DC electrical circuits. Since vascular resistance is inversely proportional to volume flux, it represents an opposition to blood flow, just as an electrical resistor opposes current. Vascular resistance is applicable to steady-state systems just as Ohm's law is only applicable to DC circuits. However, flows with a periodic component, such as those encountered during vasomotion, always have a steady-state component, namely the mean flow, to which the concept of vascular resistance can be applied [24].

Funk et al. [8] used a mathematical model to show that vascular resistance decreases as the amplitude of vasomotion increases. However, observations from experiments appear to suggest the opposite. Meyer et al. [22] observed that vasomotion was reduced in isolated resistance arteries from the mesenteric circulation of pregnant rats compared to those of non-pregnant rats. Pregnancy is associated with low vascular resistance [11]. In addition, isolated arteries exhibit increased vasomotion in preeclampsia [5], which is an abnormal state of high resistance during pregnancy. Finally, increased vasomotion has been observed in animal models of increased vascular resis-

tance [22]. Motivated by these observations, Gratton et al. [11] revisited the modeling of Funk et al. [8], and showed that vascular resistance increases with vasomotion, consistent with experimental observations and in accordance with the earlier modeling work of Parthimos et al. [26].

The contradictory results are resolved in Chapter 2 and an explanation is given as to why Funk et al. [8] are correct with their analysis. An argument is provided that resolves the apparent inconsistency between theoretical predictions and experimental observations. In addition, the validity of the use of Poiseuille's law in computing vascular resistance is examined.

The second part of the thesis, contained in Chapters 3 and 4, deals with a mathematical model of the electrophysiology that regulates intracellular calcium concentration and the corresponding production of muscle stress. Several mathematical models have already been developed to model either the myogenic response or vasomotion [16, 27, 33]. The shortcoming of these models is that they do not consider the role of intracellular calcium, which is the primary stimulus for smooth muscle contraction.

The focus of Chapter 3 is to review a model by Gonzalez-Fernandez and Ermentrout [10] on the origin and dynamics of vasomotion. This model incorporates intracellular calcium concentration by coupling the Morris-Lecar [23] model that describes the electrophysiology of the barnacle giant muscle fiber with the mechanical properties of vascular smooth muscle. In Chapter 4, the model is extended to account for the myogenic response and the maintenance of myogenic tone. In Chapter 5, the purpose and conclusions of the thesis

are discussed.

Chapter 2

Effect of vasomotion on vascular resistance

Blood flow through vessels is similar to fluid flow through rigid pipes. Although blood is a non-Newtonian fluid and the vessel wall is elastic [24], the mathematics that describe fluid flow through pipes can still be applied to blood flow. Poiseuille's law is a well-accepted formula to calculate the volume flux in rigid pipes, and is often referred to when discussing vascular resistance and blood flow in blood vessels. The derivation of Poiseuille's law and the assumptions on which it is based are reviewed in Section 2.1. In Section 2.2, the calculations that lead to the controversy on the effect of vasomotion on vascular resistance are reviewed, and the controversy is resolved. The calculations of vascular resistance rely on the use of Poiseuille's law, even though some of the assumptions underlying it are violated. Conditions under

which the applicability of Poiseuille's law is valid are analyzed in Section 2.3. In Section 2.4, the physiological significance of the results are discussed.

2.1 Poiseuille's law

Poiseuille's law for pipe flow is often referred to when discussing blood flow in vessels. Poiseuille's law gives the fluid volume flux through a tube as a function of the pressure gradient, fluid viscosity, and pipe radius.

Poiseuille was a French physician who was interested in capillary flow. Due to the difficulty of blood clotting when exposed to air, Poiseuille was forced to experiment with water flow through glass tubes of capillary size. Nonetheless, it was sometime in the 1840s when he experimentally obtained the relationship,

$$F = K \frac{\Delta p}{L} r_0^4, \quad (2.1)$$

where F , Δp , L , and r_0 are volume flux, pressure drop, pipe length, and pipe radius, respectively. The constant K was determined under a variety of conditions, and is actually representative of the fluid viscosity [24].

It was Wiedemann in 1856 and Hagenbach in 1860 who independently derived Poiseuille's law on theoretical grounds [24]. The derivation that follows here is slightly more complicated than their derivation, but is presented to later justify the applicability of Poiseuille's law to vasomotion.

The Navier-Stokes equations are the equations of motion for fluid flow.

In cylindrical coordinates, a fluid velocity field $\mathbf{u} = (u_r, u_\theta, u_x)$ satisfies

$$\begin{aligned}\frac{\partial u_r}{\partial t} + (\mathbf{u} \cdot \nabla) u_r - \frac{u_\theta^2}{r} &= -\frac{1}{\rho} \frac{\partial p}{\partial r} + \nu \left(\nabla^2 u_r - \frac{u_r}{r^2} - \frac{2}{r^2} \frac{\partial u_\theta}{\partial \theta} \right), \\ \frac{\partial u_\theta}{\partial t} + (\mathbf{u} \cdot \nabla) u_\theta + \frac{u_r u_\theta}{r} &= -\frac{1}{\rho r} \frac{\partial p}{\partial \theta} + \nu \left(\nabla^2 u_\theta + \frac{2}{r^2} \frac{\partial u_r}{\partial \theta} - \frac{u_\theta}{r^2} \right), \\ \frac{\partial u_x}{\partial t} + (\mathbf{u} \cdot \nabla) u_x &= -\frac{1}{\rho} \frac{\partial p}{\partial x} + \nu \nabla^2 u_x,\end{aligned}\tag{2.2}$$

with

$$\begin{aligned}\mathbf{u} \cdot \nabla &= u_r \frac{\partial}{\partial r} + \frac{u_\theta}{r} \frac{\partial}{\partial \theta} + u_x \frac{\partial}{\partial x}, \\ \nabla^2 &= \frac{1}{r} \frac{\partial}{\partial r} \left(r \frac{\partial}{\partial r} \right) + \frac{1}{r^2} \frac{\partial^2}{\partial \theta^2} + \frac{\partial^2}{\partial x^2},\end{aligned}$$

where ρ and ν are the fluid density and kinematic viscosity respectively [21]. The Navier-Stokes equations are very difficult to work with due to the non-linearity of the system. However, the system can be significantly simplified with the following assumptions for pipe flow:

1. The radius of the pipe is constant at $r = r_0$,
2. the velocity profile is one dimensional in the x direction such that $\mathbf{u} = (0, 0, u_x)$,
3. the system has reached steady-state such that $\frac{\partial \mathbf{u}}{\partial t} = 0$,
4. there exists a no-slip boundary condition such that $u_x(r_0) = 0$,
5. the fluid is incompressible such that $\nabla \cdot \mathbf{u} = 0$, and
6. the fluid velocity is finite.

These assumptions simplify (2.2) to

$$-\frac{dp}{dx} + \frac{\mu}{r} \frac{d}{dr} \left(r \frac{du_x}{dr} \right) = 0,$$

with $\mu = \rho\nu$, which can be solved for u_x with the above boundary conditions to give,

$$u_x = \frac{r^2 - r_0^2}{4\mu} \frac{dp}{dx}. \quad (2.3)$$

Equation (2.3) shows a parabolic velocity profile. The volume flux is evaluated by integrating the fluid velocity over the cross-sectional area of the pipe to get

$$\begin{aligned} F &= 2\pi \int_0^{r_0} u_x dr \\ &= -\frac{\pi r_0^4}{8\mu} \frac{dp}{dx}. \end{aligned}$$

By letting $\frac{dp}{dx} = -\frac{\Delta p}{L}$, this is rewritten as

$$F = \frac{\pi \Delta p}{8 \mu L} r_0^4, \quad (2.4)$$

which is Poiseuille's law. This is in agreement with the qualitative result by Poiseuille given in (2.1), with $K = \frac{\pi}{8\mu}$.

2.2 Background, setup, and analysis of the model

Poiseuille's law, (2.4), was derived in the last section since it is used in the calculation of the effect of vasomotion on vascular resistance, which is defined in (1.1) on page 3. Combining equations (1.1) and (2.4) gives the following expression for the vascular resistance as a function of the vessel radius r :

$$R_V = \frac{8 \mu L}{\pi r^4}. \quad (2.5)$$

This relationship is the starting point for the mathematical modeling by Funk et al. [8], Gratton et al. [11], and Parthimos et al. [26].

Vasomotion is exhibited in a large variety of patterns [32]. A common pattern is sinusoidal in nature, and hence the following form for r in (2.4) and (2.5) is assumed [8, 11, 26]:

$$r = r(t) = r_0(1 + \lambda \sin \omega t), \quad (2.6)$$

where r_0 , λ , ω and t is the average vessel radius, the fractional amplitude of oscillation ($\lambda < 1$), the frequency of oscillation, and time, respectively. The time-dependence of r in (2.6) immediately violates the steady-state definition of vascular resistance, (1.1), and the assumption of time-independence in Poiseuille's law, (2.4). However, under certain conditions (which are explained in Section 2.3), it is reasonable to use Poiseuille's law as an approxi-

mation for the time-dependent volume flux.

Assuming for the moment that Poiseuille's law is applicable, the average volume flux over one period of oscillation is given by

$$\bar{F} = \frac{\omega}{2\pi} \int_0^{\frac{2\pi}{\omega}} F(t) dt, \quad (2.7)$$

where $\frac{2\pi}{\omega}$ is the period of oscillation from (2.6), and $F(t) = \frac{\pi \Delta p}{8 \mu L} [r(t)]^4$.

Evaluating the integral gives

$$\bar{F} = \frac{\pi \Delta p}{8 \mu L} \left(1 + 3\lambda^2 + \frac{3}{8}\lambda^4 \right) r_0^4. \quad (2.8)$$

The average volume flux is normalized with respect to a vessel without vasomotion to give

$$\hat{F} = \frac{\bar{F}}{\bar{F}|_{\lambda=0}} = \left(1 + 3\lambda^2 + \frac{3}{8}\lambda^4 \right), \quad (2.9)$$

as was obtained by Parthimos et al. [26]. Note that $\bar{F}|_{\lambda=0} = F$ as given in (2.4). Thus, the normalized volume flux, \hat{F} , increases with an increase of vasomotion amplitude, λ , as shown in Figure 2.1(a).

It would seem appropriate to evaluate an integral similar to (2.7) to calculate the time average of vascular resistance, as follows:

$$\bar{R}_V = \frac{\omega}{2\pi} \int_0^{\frac{2\pi}{\omega}} R_V(t) dt, \quad (2.10)$$

where $R_V(t) = \frac{8}{\pi} \frac{\mu L}{[r(t)]^4}$. Evaluating the resulting integral, and normalizing

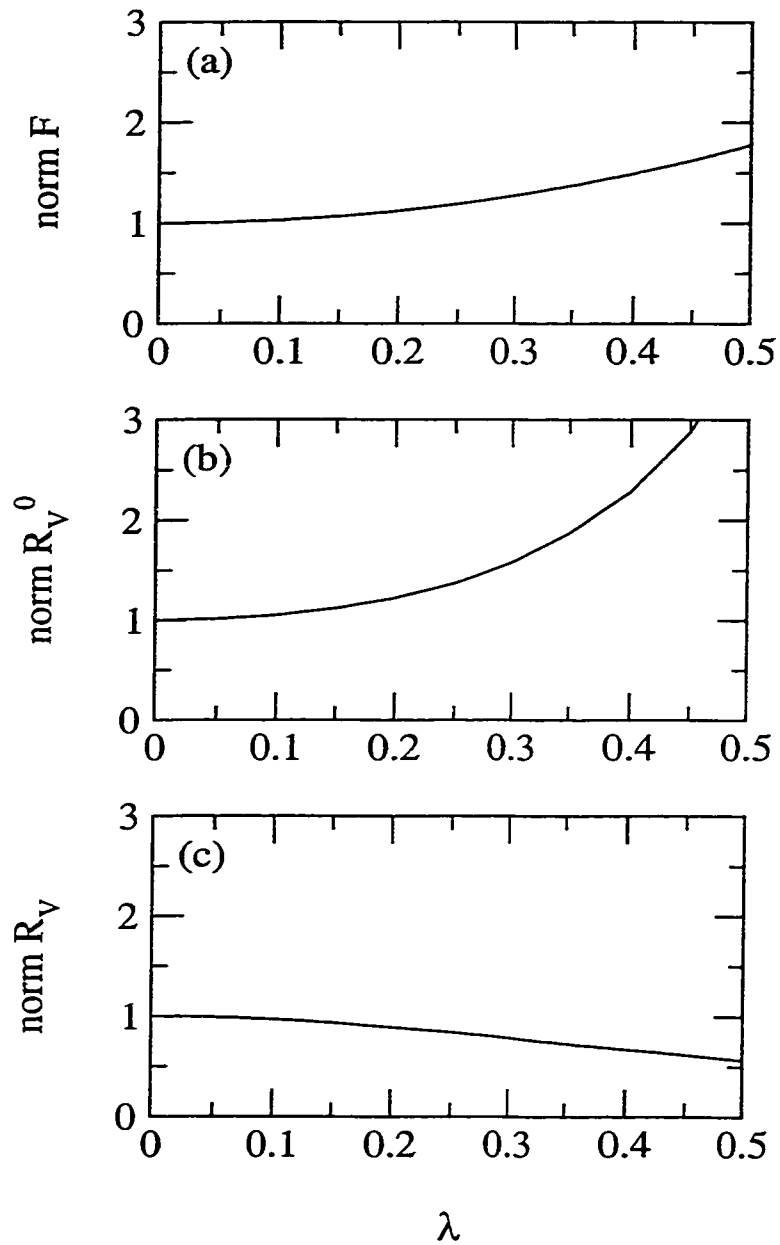


Figure 2.1: (a) Normalized volume flux, (2.9), as a function of vasomotion amplitude, λ . (b) Normalized vascular resistance, (2.11), as a function of λ . (c) Normalized effective vascular resistance, (2.14), as a function of λ .

with respect to a vessel without vasomotion gives

$$\hat{R}_V^0 = \frac{\bar{R}_V}{\bar{R}_V|_{\lambda=0}} = \frac{3\lambda^2 + 2}{2(1 - \lambda^2)^{\frac{1}{2}}}. \quad (2.11)$$

This is the result of Gratton et al. [11] and Parthimos et al. [26]. Figure 2.1(b) gives the graph of \hat{R}_V^0 as a function of λ , which shows that \hat{R}_V^0 increases with an increase in λ .

However, these results are inconsistent since time-averaged volume flux, (2.9), and time-averaged vascular resistance, (2.11), cannot both increase with λ as it contradicts the definition of vascular resistance, (1.1). Parthimos et al. [26] recognized this paradox but did not resolve it.

The problem arises in the calculation of the average vascular resistance in (2.10). The definition of vascular resistance given in (1.1) on page 3 applies to steady-state flows or to the steady-state component of the flow (i.e., mean flow). Therefore, the definition of vascular resistance must be applied directly to the mean flow (2.7) to give the effective vascular resistance

$$\bar{R}_V = \frac{\Delta p}{\bar{F}}, \quad (2.12)$$

or equivalently,

$$\begin{aligned} \bar{R}_V &= \frac{\Delta p}{\frac{\omega}{2\pi} \int_0^{2\pi} F(t) dt} \\ &= \frac{1}{\frac{\omega}{2\pi} \int_0^{2\pi} \frac{1}{R_V(t)} dt}. \end{aligned} \quad (2.13)$$

Equation (2.13) is just the continuous harmonic mean of $R(t)$. Although (2.10) is the time-averaged vascular resistance, it is not representative of the effective vascular resistance. Furthermore, calculating the time-averaged vascular resistance makes no physical sense since vascular resistance is not a rate, but a quantity with units $dyne \cdot s/cm^5$.

Using equation (2.8) in equation (2.12), and normalizing as before gives,

$$\hat{R}_V = \frac{\bar{R}_V}{\bar{R}_V|_{\lambda=0}} = \frac{1}{1 + 3\lambda^2 + \frac{3}{8}\lambda^4} \quad (2.14)$$

Figure 2.1(c) shows \hat{R}_V as a function of λ . Effective vascular resistance decreases with an increase of vasomotion amplitude, λ , as consistent with the definition. This is the conclusion of Funk et al. [8], and the one that is correct.

The discussion on the physiological significance of this result is postponed to section 2.4. In the following section, the applicability of Poiseuille's law for a time-dependent situation such as vasomotion is analyzed.

2.3 The use of Poiseuille's law in modeling the effect of vasomotion on vascular resistance

Poiseuille's law is based on the assumption that the flow has reached steady state. In the model discussed in the previous section, the radius r in

Poiseuille's law depends on time according to equation (2.6). By continuing the use of Poiseuille's law, the flow rate is assumed to instantaneously reflect the current radius at all times. However, a lag is introduced as it takes time for the flow to adjust to the changing radius, which is a consequence of the fluid inertia.

This section examines conditions under which lag effects are minimal and the use of Poiseuille's law yields a reasonable approximation to the flow rate of a vessel with an oscillating radius. Three arguments are presented in Sections 2.3.1, 2.3.2, and 2.3.3.

2.3.1 Argument 1 - Slow varying wall radius

Lag effects are minimized if the velocity of the changing radius is small in comparison to the characteristic fluid velocity. For the sinusoidal radius assumed in equation (2.6), the magnitude of the rate of change of $r(t)$ is

$$|r'(t)| = |r_0\lambda\omega \cos \omega t| \leq r_0\lambda\omega. \quad (2.15)$$

The magnitude of the wall velocity, $r'(t)$, is bounded by the product $r_0\lambda\omega$. To determine whether this product is sufficiently small, it is compared to the characteristic fluid velocity through a static pipe with radius r_0 , given by $\bar{u}_x = \frac{F}{\pi r_0^2}$, where F is the volume flux as before. The ratio of these two velocities give the nondimensional number $D = \frac{r_0\lambda\omega}{\bar{u}_x} = \frac{r_0^3\lambda\omega\pi}{F}$. If $D \ll 1$, then the wall velocity is significantly less than the characteristic fluid velocity and

lag effects will be negligible. On the other hand, if $D \ll 1$ is not satisfied, then more complex analysis is required. For the vessels of interest, typical parameter values are $r_0 = 225 \mu\text{m}$, $\lambda = 0.02$, $\frac{\omega}{2\pi} = 0.375 \text{ Hz}$, and $F = 100 \mu\text{L}/\text{min}$ (see [32] for example). With these values, $D \approx 10^{-3} \ll 1$. Even if the amplitude of the vasomotion is much larger than $\lambda = 0.02$, D still remains sufficiently small.

2.3.2 Argument 2 - Stokes number

The steady-state assumption, $\frac{\partial \mathbf{u}}{\partial t} = 0$, made in Section 2.1 cannot be made for fluid flow in vasomotion. Furthermore, a radial velocity component is introduced such that $\mathbf{u} = (u_r, 0, u_x)$. A thorough analysis of the Navier-Stokes equations under these conditions becomes very complex and difficult. However, the system can be simplified by dropping negligible terms.

Recall from Section 2.1 that the derivation of Poiseuille's law is based on the x -component of the Navier-Stokes equations (2.2) in cylindrical coordinates. This equation is the differential form of the following force-balance equation:

$$\begin{pmatrix} \text{transient} \\ \text{inertia} \end{pmatrix} + \begin{pmatrix} \text{convective} \\ \text{inertia} \end{pmatrix} = \begin{pmatrix} \text{pressure} \\ \text{force} \end{pmatrix} + \begin{pmatrix} \text{viscous} \\ \text{force} \end{pmatrix}.$$

The transient inertia term cannot be dropped since the system is not steady state. However, nondimensionalization can yield conditions under which the

transient inertia term can be safely neglected. Introduce the following nondimensional variables,

$$\begin{aligned}x &= L\hat{x}, & \mathbf{u} &= U\hat{\mathbf{u}}, \\p &= \rho U^2 \hat{p}, & t &= \frac{\hat{t}}{\omega},\end{aligned}$$

where L , U , and ω are characteristic length, velocity, and frequency. Substitute into the x -component of (2.2), rearrange, and drop the hats to get,

$$\frac{\omega L}{U} \frac{\partial u_x}{\partial t} + (\mathbf{u} \cdot \nabla) u_x = -\frac{\partial p}{\partial x} + \frac{\nu}{UL} \nabla^2 u_x.$$

The non-dimensional number $R = \frac{UL}{\nu}$ is known as *Reynolds number*. Under steady-state conditions ($\frac{\partial \mathbf{u}}{\partial t} = 0$), the magnitude of R gives insight into whether the flow is dominated by viscous forces ($R \ll 1$) or convective inertia ($R \gg 1$).

Further arranging of the terms gives

$$\frac{\omega L^2}{\nu} \frac{\partial u_x}{\partial t} + \frac{UL}{\nu} (\mathbf{u} \cdot \nabla) u_x = -\frac{UL}{\nu} \frac{\partial p}{\partial x} + \nabla^2 u_x.$$

The non-dimensional number $N_s = \frac{\omega L^2}{\nu}$ is known as *Stokes number*. The Stokes number gives insight into whether the flow is dominated by transient inertia or by viscous forces. If the Stokes number is sufficiently small ($N_s \ll 1$), then the transient inertia term of the Navier-Stokes equation can be dropped, leaving the steady-state equation from which Poiseuille's law can be derived as in Section 2.1. Although there exists a u_r velocity component, it can be safely neglected by the argument given in Section 2.3.1.

For typical vasomotion in resistance vessels, the characteristic frequency and length are the frequency of oscillation and the average radius of the vessel, respectively. Typical values are $\nu = 0.04 \text{ cm}^2/\text{s}$ [24], $\omega = 1.67 \text{ rad/s}$ [12] and $L = 200 \text{ }\mu\text{m}$. These values give a Stokes number of $N_s = 0.0167$, sufficiently small to drop the transient term, as desired.

2.3.3 Argument 3 - Fast transient to a similar problem

Brodkey [3] considered a fluid flow problem very similar to that of Poiseuille flow. The setup of the system is the same, except the fluid is at complete rest at $t = 0$. As $t \rightarrow \infty$, the system approaches the steady-state parabolic velocity profile given by equation (2.3).

The interesting part of the solution is the speed at which the system approaches the steady-state solution. If the transient is very fast, then it is reasonable to assume that vasomotion flow will adjust quickly to the changing radius, such that Poiseuille's law essentially gives the instantaneous volume flux at any moment. The details of the procedure used to obtain the solution are provided in [3], with a final result of

$$u_x = -\frac{r_0^2}{4\mu} \frac{dp}{dx} \left[1 - \frac{r^2}{r_0^2} - 8 \sum_{n=1}^{\infty} \frac{J_0\left(\frac{\alpha_n r}{r_0}\right)}{\alpha_n^3 J_0'(\alpha_n)} e^{-\alpha_n^2 \frac{\nu t}{r_0^2}} \right], \quad (2.16)$$

where α_n is the n^{th} root of the Bessel function J_0 ($J_0(\alpha_n) = 0$). The summation in (2.16) is the transient term which decays to zero as $t \rightarrow \infty$. The rate at which decay occurs is determined by the exponential. By picking a

characteristic time scale of $t = \frac{\hat{t}}{\omega}$, the requirement for the transient solution to decay quickly is that $\frac{\nu}{r_0^2 \omega}$ be large. However, this number is just the inverse of the Stokes number, N_s , as discussed in Section 2.3.2. In that section, N_s was required to be small. This is the same as $\frac{1}{N_s}$ being large, as desired here.

2.4 Discussion

The calculated effect of vasomotion on vascular resistance given by (2.14) shows that effective vascular resistance decreases with an increase of vasomotion. This results seems inconsistent with experimental observations. Decreased vasomotion is observed in low-resistance physiological states (e.g., pregnancy), and increased vasomotion is observed in high-resistance physiological states (e.g., preeclampsia and hypertension) [11]. In this section, the apparent disagreement between the theoretical results and the experimental observations are resolved.

Recall that the quantities \hat{F} and \hat{R}_V , given by (2.9) and (2.14), respectively, have been normalized relative to a similar vessel with a vasomotion amplitude of zero ($\lambda = 0$). The shortcoming of this normalization is that the dependence on the mean radius, r_0 , has been dropped. In fact, the average radius of a mesenteric artery in pregnancy is increased at the same time as vasomotion amplitude is decreased. Similarly, the average radius of a mesenteric artery in preeclampsia and hypertension is reduced while vasomotion amplitude is increased. Due to the r_0^4 dependence, blood flow and vascular

resistance have a much greater dependence on the mean radius than on the amplitude of vasomotion. For example, if the average radius of oscillation is increased by just 19%, the effective vascular resistance is decreased by 200%. It is therefore insufficient to only consider changes in the amplitude of vasomotion when comparing different physiological conditions such as pregnancy and hypertension.

Slaaf et al. [31] suggest that it is misleading to focus only on vasomotion amplitude and average radius. There is a complicated interplay between these factors, in addition to the pattern of vasomotion which may not be sinusoidal as assumed in most of the modeling studies. It is possible that two vessels with different combinations of average radius and vasomotion amplitude may have the same effective vascular resistance and hence the same flow-carrying capacity. For example, a vessel with mean radius $r_0 = 9.31 \mu\text{m}$ and vasomotion amplitude $\lambda = 0.4$ has essentially the same effective vascular resistance as a vessel with $r_0 = 10.00 \mu\text{m}$ and $\lambda = 0.2$. Slaaf et al. [31] introduce the notion of an ‘effective radius’ to facilitate comparison of different vessels. The effective radius is defined to be radius of a fictitious static vessel that has the same vascular resistance and the flow-carrying capacity as the vessel undergoing vasomotion, and takes into account the particular pattern of vasomotion.

This chapter was motivated by the contradictory results by Funk et al. [8], who showed that vascular resistance decreases with vasomotion, and Gratton et al. [11] and Parthimos et al. [26], who showed the opposite, namely that

vascular resistance increases with vasomotion. The contradiction is resolved by a careful look at the meaning of vascular resistance. It is shown that the result obtained by Funk et al., namely that vascular resistance decreases with vasomotion, is correct. This implies that vasomotion contributes to flow. It is also suggested that comparing vessels by the amplitude of the vasomotion alone is misleading, and can lead to apparent inconsistencies between theory and experimental observations. To correctly compare the vascular resistance or, equivalently, the flow-carrying capacity of different vessels, the use of an 'effective radius' is advocated. The effective radius takes into account the amplitude, pattern, and mean radius of the vasomotion.

Chapter 3

A mathematical model of smooth muscle activity

In 1994, Gonzalez-Fernandez and Ermentrout [10] developed the first dynamical model of vasomotion that took into consideration the electrophysiology of smooth muscle. In this chapter, the derivation of the model is reviewed. The equations presented here are modified slightly from the original ones. The modifications are based on the model of Ursino et al. [33] and a simplified model of Gonzalez-Fernandez [9].

What is unique about this model is that it takes into account the transport of ions across the membrane of the smooth muscle cells and the dynamics of the intracellular calcium concentration. These factors are neglected in other mathematical models of smooth muscle activity [16, 27, 33]. In all, the model takes into account the transport of ions across the cell membrane,

the transmural pressure, the wall elastic and smooth muscle stresses, and the associated vessel contraction or dilation [10]. This is accomplished by using the well-known Morris-Lecar [23] model for the electrophysiology of the barnacle giant muscle fiber, and combining it with the mechanical properties of smooth muscle.

The derivation of the model is given in Section 3.1. The model is summarized in Section 3.2 and briefly analyzed in Section 3.3. A discussion of the results and the validity of the assumptions used in the derivation is given in Section 3.4.

3.1 Model derivation

The first three equations of the model are based on the Morris-Lecar [23] model. These equations are independent of the rest of the system, and describe the smooth muscle cell membrane potential, the fraction of open potassium channels, and the intracellular calcium concentration.

It is well known that intracellular calcium is the primary stimulus of muscle contraction. Since intracellular calcium concentration can qualitatively predict steady-state muscle stress [28], the fourth differential equation of the model describes the dynamic dependence of muscle contraction on the intracellular calcium concentration. The known muscle stress is used in the fifth equation which models the dynamics of the actual vessel radius by balancing the hoop forces in the vessel wall.

The mechanics of smooth muscle is presented in Section 3.1.1. The mathematical equations which determine muscle activation are given in Section 3.1.2, followed by the equations for the electrophysiology and calcium concentration in Section 3.1.3.

3.1.1 Smooth muscle mechanics

The model assumes the balance of four forces to determine the vessel radius. These forces are

1. transmural pressure, $f_{\Delta p}$,
2. internal wall friction, f_f ,
3. elastic force (inactive), f_e , and
4. muscle force (active), f_c .

These forces are described in Sections 3.1.1.1 - 3.1.1.4, respectively, and the complete force balance equation is given in Section 3.1.1.5.

3.1.1.1 Transmural pressure force

Laplace's law relates the tension (force per unit length) in the vessel wall, $T_{\Delta p}$, to the radius and the transmural pressure as follows [24]:

$$T_{\Delta p} = \Delta p \cdot r_i,$$

where Δp and r_i are the transmural pressure and inner vessel radius, respectively. Note that the transmural pressure, Δp , is not the same as the intraluminal pressure used in Poiseuille's law in (2.4). The transmural pressure is the pressure drop between the inside and the outside of the vessel. The cross-sectional area of the vessel wall, A , is assumed to remain constant such that

$$A = \pi (r_o^2 - r_i^2)$$

is constant with r_o being the outer vessel radius. By letting $r = \frac{r_o + r_i}{2}$ be the average vessel radius, the tension in the vessel wall can be written as

$$T_{\Delta p} = \Delta p \left(r - \frac{A}{4\pi r} \right),$$

where $r > \sqrt{\frac{A}{4\pi}}$. This is multiplied by a unit length, L , to give the force due to the transmural pressure, $f_{\Delta p}$, as a function of the radius and transmural pressure,

$$f_{\Delta p} = \Delta p \left(r - \frac{A}{4\pi r} \right) \cdot L. \quad (3.1)$$

3.1.1.2 Internal wall friction force

The internal wall friction force, f_f , is assumed to be linearly proportional to the wall velocity,

$$f_f = \tau \frac{dr}{dt}, \quad (3.2)$$

with τ constant.

3.1.1.3 Vessel elastic force

The elastic properties of the vessel are determined experimentally under conditions where the muscle is completely inactive. Stress is applied to the vessel wall by increasing the transmural pressure and measuring the corresponding radius. The shape of the stress-radius curve is roughly consistent between vessels, and is normalized with respect to the stress, σ_0 , and radius, r_{ref} , at which maximum muscle stress occurs (reviewed in Section 3.1.1.4). The resulting curve is shown in Figure 3.1, and the relationship is modeled by an exponential function of the following form [33]:

$$\sigma_e(r_n) = \sigma_{e0} \left[e^{k_e(r_n - r_0)} - 1 \right],$$

with k_e , σ_{e0} , and r_0 constant, and $r_n = \frac{r}{r_{ref}}$. This function is simpler than the one used by Gonzalez-Fernandez and Ermentrout [10], but has roughly the same shape. The total elastic hoop force, f_e , on a longitudinal section of the vessel wall with area S is given by [10]

$$f_e = S \cdot \sigma_e(r_n) \cdot \sigma_0, \tag{3.3}$$

where σ_0 is the maximum stress produced by the muscle.

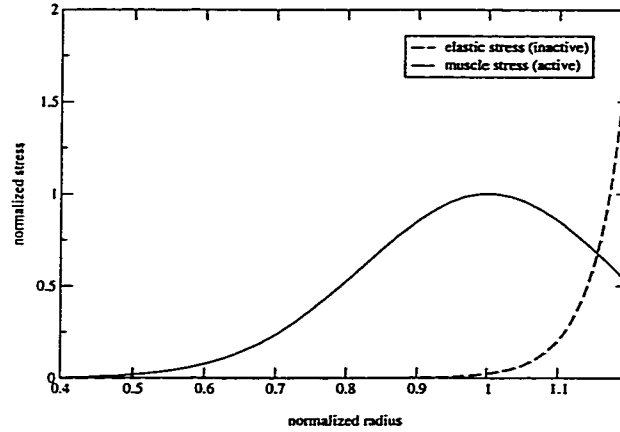


Figure 3.1: Artery normalized stress versus normalized radius. The dotted curve represents the elastic component of stress for the vessel. The solid curve represent the muscle stress component for the vascular smooth muscle for a given radius at maximum contraction.

3.1.1.4 Muscle contraction force

Muscle stress is experimentally determined in a similar manner to the elastic stress given in Section 3.1.1.3, except under conditions where the muscle is at maximum contraction. To obtain the stress-radius curve for muscle contraction alone, the elastic component from Section 3.1.1.3 is subtracted. The resulting stress-radius curve is bell shaped and is normalized with respect to the stress and radius at which maximum muscle stress occurs. The resulting curve is shown in Figure 3.1, and the relationship is modeled by [33]

$$\sigma_c(r_n) = e^{-k_c(r_n - r_c)^2},$$

with k_c and r_c constant. The constant r_c is the normalized radius at which maximum stress production occurs ($r_c = 1$). Again, this function is simpler

than the one used by Gonzalez-Fernandez and Ermentrout [10], but has a similar shape.

Smooth muscle can also be in a state of partial contraction. To accommodate for this state, define ω to be the fraction of activation of muscle such that $\omega = 0$ denotes no muscle stress production and $\omega = 1$ denotes maximum muscle contraction. The value of ω is determined by the current physiological state of the vessel which is reviewed in Sections 3.1.2 and 3.1.3.

The total muscle contraction hoop force, f_c , on a longitudinal section of the vessel wall with area S is given by [10]

$$f_c = S \cdot \sigma_c(r_n) \cdot \sigma_0 \cdot \omega, \quad (3.4)$$

with σ_0 as defined before in Section 3.1.1.3.

3.1.1.5 Net force

By Newton's Law, the sum of the forces acting on a free body is equal to zero. Adding the forces from (3.1), (3.2), (3.3), and (3.4) according to the free-body diagram shown in Figure 3.2 gives

$$f_{\Delta p} - f_e - f_c - f_f = 0.$$

This equation can be solved for $\frac{dr}{dt}$ (from (3.2)) to give

$$\frac{dr}{dt} = \frac{1}{\tau} (f_{\Delta p} - f_e - f_c). \quad (3.5)$$

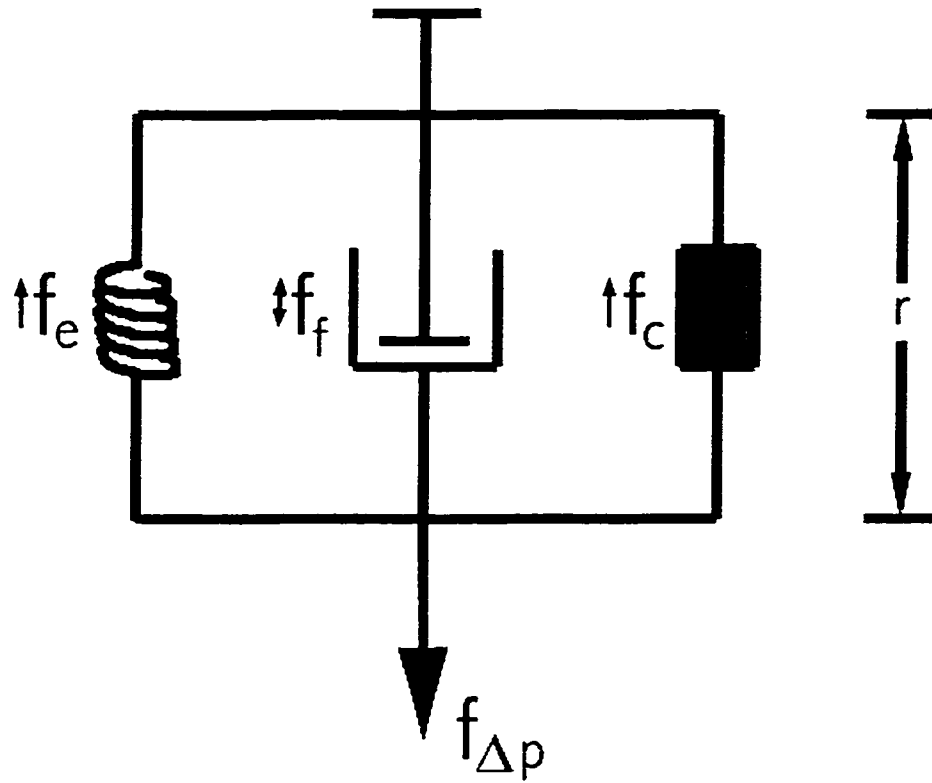


Figure 3.2: Free body diagram of forces assumed in the vessel wall.

Equation (3.5) is the fifth equation of the model.

The next section discusses the physiology involved in determining the muscle activation, ω , and the mathematical model used to describe the dynamics of ω .

3.1.2 Muscle stress development and the dependence on intracellular calcium

Within smooth muscle cells are thick and thin filaments which are responsible for stress production. These filaments overlap in a longitudinal fashion. It is the interaction between the thick and thin filaments (sliding filament theory) that is believed to be responsible for stress production [29].

Thin filaments are made up of globular protein molecules called *actin*. Actin molecules are about 5.5 nanometers in diameter and are joined end-to-end to form a long structure resembling a chain of beads. These chains are wound in pairs to produce helical shaped thin filaments [29].

Thick filaments are made up of large protein molecules called *myosin*. A myosin molecule has a long rod-shaped section (sometimes called the tail section) with a double globular head. Attached to the globular heads are two protein molecules called *light chains*. About 300-400 myosin molecules bundled together by the tails make up a thick filament. Protruding from the sides of the bundle are the double globular heads which are referred to as *crossbridges*. It is the interaction of the crossbridges on the thick filament with the actin on the thin filament that is the cause of stress production [29]. The physical relationship between thin and thick filament are illustrated in Figure 3.3.

Shortening of the muscle is brought about by a cyclic “rowing” motion of the crossbridges, in which they successively attach to the closest available

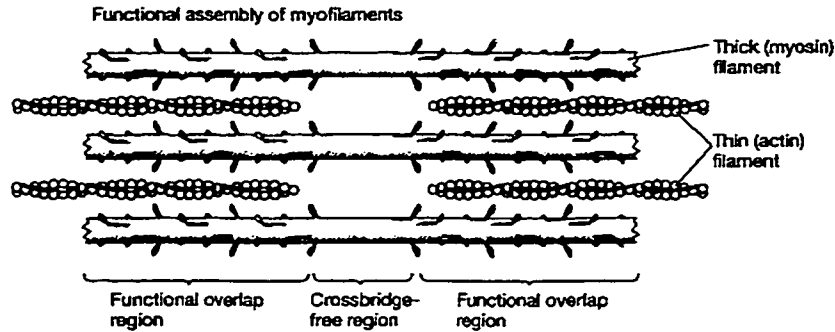


Figure 3.3: Diagram of overlapping thick and thin filaments. Figure taken from Rhoades et al. [29].

thin filament site, change their shape and pull the actin filament along, then let go of the actin and reattach further along [29]. A prerequisite for the myosin to bind to actin is the phosphorylation of the myosin head light chain. Phosphorylation depends on the presence of free intracellular calcium, as follows.

Free intracellular calcium combines with calmodulin which in turn activates the myosin light chain kinase (MLCK) enzyme. It is the activation of this enzyme which allows the phosphorylation of the light chains which leads to crossbridge cycling and muscle contraction.

The dependence of myosin phosphorylation on calcium is assumed as follows. Let ψ be the fraction of phosphorylated myosin light chains ($0 \leq \psi \leq 1$). Steady-state phosphorylation is experimentally shown to have a sigmoidal dependence on intracellular calcium concentration, Ca_i :

$$\psi = \frac{Ca_i^q}{Ca_{im}^q + Ca_i^q}, \quad (3.6)$$

with q constant, and Ca_{im} being the reference calcium level at which half of the myosin light chains are phosphorylated [28]. The value for Ca_{im} is believed to be modulated by agonists. Changing this parameter essentially alters the sensitivity of myosin phosphorylation on the free intracellular calcium concentration. The dependence of the model dynamics on Ca_{im} is further developed in Chapter 4 with regard to the regulation of myogenic tone.

Once a myosin light chain becomes phosphorylated, it can react with actin to form crossbridge cycling. The dependence of the fraction of attached crossbridges, ω , on ψ is modeled as follows [10]:

$$\frac{d\omega}{dt} = k_\psi \left(\frac{\psi}{\psi_m + \psi} - \omega \right), \quad (3.7)$$

where k_ψ is a rate constant, and ψ_m is constant. Equation (3.7) is such that ω approaches $\frac{\psi}{\psi_m + \psi}$ at a rate determined by k_ψ . The variable ω gives meaning to muscle activation. If all the phosphorylated light chains are forming crossbridges, then $\omega = 1$. Similarly, if none of the myosin light chains are phosphorylated, then no crossbridge cycling can occur and $\omega = 0$. It is ω that determines the muscle activation in equation (3.4).

Since the phosphorylation of the myosin light chains depends on the intracellular calcium concentration, an equation that determines intracellular calcium concentration is required. Such an equation is developed in the next section.

3.1.3 Electrophysiology and intracellular calcium concentration of vascular smooth muscle

The primary mechanism for extracellular calcium to enter the cell is via the voltage-dependent calcium channels, which are distributed within the cell membrane. The extrusion of intracellular calcium is assumed to occur via ATP pumps, also distributed within the cell membrane. Thus, the following equation models the dynamics of the free intracellular calcium concentration:

$$\frac{dCa_i}{dt} = [-\alpha I_{Ca} - k_{Ca} Ca_i] \rho. \quad (3.8)$$

Here, the influx of intracellular calcium is represented by $-\alpha I_{Ca}$. I_{Ca} is the membrane current which results from the transport of calcium ions into the cell and α is the conversion factor from the ionic current to the molar rate of calcium ions. The extrusion of calcium from the ATP pump is assumed to be first order with rate constant k_{Ca} [10].

The factor ρ takes into account the existence of intracellular buffers for the calcium ions. The presence of buffers means that most calcium ions entering the cell are bound to free radicals. It is only a small fraction of the calcium ions (given by ρ) that remains available for cellular functions. The amount of free intracellular calcium depends on the amount of buffer, B_T , and the dissociation constant, K_d , for binding of calcium to the buffer. The functional dependence of ρ on Ca_i is derived by Gonzalez-Fernandez and

Ermentrout [10] and is given by

$$\rho = \frac{(K_d + Ca_i)^2}{(K_d + Ca_i)^2 + K_d B_T}.$$

To complete the model, an equation which describes the calcium current, I_{Ca} , is required. In order to do so, the flow of other ions, in particular the potassium ions, needs to be taken into account. This is done according to the Hodgkin-Huxley [15] formulation, in which the dynamics of the membrane potential are described by Kirchoff's law,

$$C \frac{dv}{dt} = -I_K - I_{Ca} - I_L, \quad (3.9)$$

where C is the membrane capacitance, and I_{Ca} , I_K , and I_L are the ionic potassium, calcium, and leak currents, respectively. The leak current is an error correction term which takes into account all membrane currents that are not directly modeled.

Ohm's law is assumed to apply to each of the currents, such that I is the product of a conductance (the inverse of electrical resistance) and a driving force. With this assumption, (3.9) is rewritten as

$$C \frac{dv}{dt} = -g_k n \cdot (v - v_k) - g_{Ca} m_\infty(v) \cdot (v - v_{Ca}) - g_l \cdot (v - v_l), \quad (3.10)$$

where g_k , g_{Ca} , and g_l are the maximum whole-cell potassium, calcium, and leak conductances, and v_k , v_{Ca} , and v_l are the corresponding Nernst poten-

tials [10]. The Nernst potential is the membrane potential at which an equilibrium of intracellular and extracellular ions exists, balanced by the chemical concentration gradient and the electrical gradient. For example, if $v = v_k$, then no transport of potassium ions through the membrane will occur. The n and $m_\infty(v)$ represent the fraction of open potassium and calcium channels, respectively. A set of channels which are partially open will result in a corresponding fraction of the maximum whole-cell membrane conductance for that channel.

The potassium and calcium channels open and close in response to the membrane potential. The fractional distribution of open calcium channels is assumed to depend instantaneously on the membrane potential and is described by [10]

$$m_\infty(v) = \frac{1}{2} \left(1 + \tanh \frac{v - v_1}{v_2} \right), \quad (3.11)$$

where v_1 and v_2 are parameters, and v is the membrane potential. A graph of $m_\infty(v)$ is shown in Figure 3.4. An influx of calcium ions causes depolarization of the membrane potential. Since $m_\infty(v)$ increases with v , this causes more calcium channels to open and further depolarization.

Voltage-dependent potassium channels behave in a similar manner to calcium. However, potassium ions flow out of rather than into the cell to cause repolarization. Potassium channels also open in response to an increase in membrane potential, which counters the positive feedback of the calcium channels. The *steady-state* fractional distribution of open potassium channels

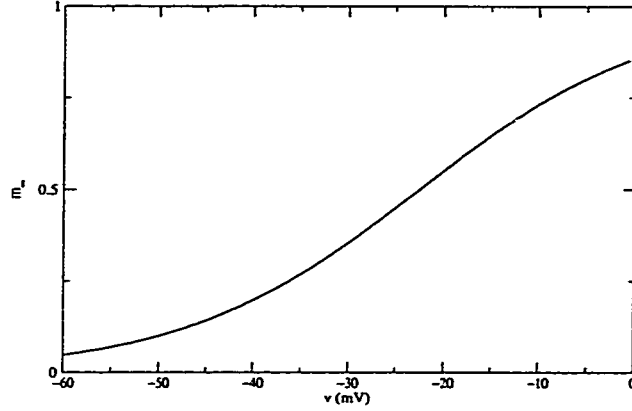


Figure 3.4: The fraction of open calcium channels, m_∞ , as a function of the membrane potential, v .

as a function of voltage is modeled by [10]

$$n_\infty(v) = \frac{1}{2} \left(1 + \tanh \frac{v - v_3}{v_4} \right).$$

Unlike the fast calcium channels, potassium channels are assumed to respond slowly to a change in membrane potential. This is modeled by letting the *actual* fraction of open potassium channels, n , be determined by,

$$\frac{dn}{dt} = \lambda_n (n_\infty(v) - n), \quad (3.12)$$

where based on statistical considerations [10],

$$\lambda_n = \phi_n \cosh \frac{v - v_3}{2v_4},$$

where ϕ_n , v_3 , and v_4 are constants.

There exists a second class of potassium channels which are sensitive to the intracellular calcium concentration. To incorporate this channel, Gonzalez-Fernandez and Ermentrout [10] let v_3 be a function of Ca_i . This effectively changes the sensitivity of n_∞ on v depending on the current calcium concentration. To simplify the analysis, v_3 is taken as constant equal to the average of v_3 over the range of Ca_i .

The differential equation (3.12) is such that n approaches n_∞ at a rate determined by λ_n . The slow potassium channel assumption is crucial for the generation of action potentials and the existence of an oscillating solution. It is this oscillation that is the driving force for vasomotion in this model. Gonzalez-Fernandez and Ermentrout [10] acknowledge that a fast potassium channel will abolish cyclic activity, and result in intermediate steady-state values for the membrane potential. Under certain experimental conditions, vessels cease to undergo vasomotion and have a constant radius. The correspondence between different physiological conditions and the different types of behaviour that can be generated by the model will be discussed further in Chapter 4.

3.2 Model summary

$$\begin{aligned} \frac{dv}{dt} = & -[g_k n \cdot (v - v_k) + g_{Ca} m_\infty(v) \cdot (v - v_{Ca}) \\ & + g_l \cdot (v - v_l)] C^{-1}, \end{aligned} \quad (3.13)$$

$$\frac{dn}{dt} = \lambda_n (n_\infty(v) - n), \quad (3.14)$$

$$\frac{dCa_i}{dt} = [-\alpha g_{Ca} m_\infty(v) \cdot (v - v_{Ca}) - k_{Ca} Ca_i] \rho, \quad (3.15)$$

$$\frac{d\omega}{dt} = k_\psi \left(\frac{\psi}{\psi_m + \psi} - \omega \right), \quad (3.16)$$

$$\frac{dr}{dt} = \frac{1}{\tau} (f_{\Delta p} - f_e - f_c), \quad (3.17)$$

with

$$n_\infty(v) = \frac{1}{2} \left(1 + \tanh \frac{v - v_3}{v_4} \right), \quad (3.18)$$

$$m_\infty(v) = \frac{1}{2} \left(1 + \tanh \frac{v - v_1}{v_2} \right), \quad (3.19)$$

$$\rho = \frac{(K_d + Ca_i)^2}{(K_d + Ca_i)^2 + K_d B_T}, \quad (3.20)$$

$$\psi = \frac{Ca_i^q}{Ca_{im}^q + Ca_i^q}, \quad (3.21)$$

$$f_{\Delta p} = \Delta p \left(r - \frac{A}{4\pi r} \right) \cdot L, \quad (3.22)$$

$$f_e = S \cdot \sigma_e(r_n) \cdot \sigma_0, \quad (3.23)$$

$$f_c = S \cdot \sigma_c(r_n) \cdot \sigma_0 \cdot \omega, \quad (3.24)$$

$$\sigma_e(r_n) = \sigma_{e0} \left[e^{k_e(r_n - r_0)} - 1 \right], \quad (3.25)$$

$$\sigma_c(r_c) = e - k_c (r_n - r_c)^2, \quad (3.26)$$

$$r_n = \frac{r}{r_{ref}}. \quad (3.27)$$

3.3 Model analysis

The vasomotion model summarized in Section 3.2 is a system of five differential equations. The analysis of the system is significantly simplified if certain dependencies are first understood. The differential equations for v and n are coupled and are independent of the remaining equations. Ca_i depends on v , ω depends on Ca_i , and r depends on ω . This is seen by

$$n \& v \Rightarrow \text{Ca}_i \Rightarrow \omega \Rightarrow r.$$

Thus, the behaviour of r is ultimately determined by the behaviour of v and n . If v and n oscillate, then the oscillation is carried through to Ca_i , ω and eventually r . The oscillation of r represents vasomotion. Similarly, if v and n are at a stable fixed point, r is also constant.

The system was numerically integrated with Bard Ermentrout's XPP software [6] on a Linux workstation. The parameters used are given in Table 3.1 and are taken from Gonzalez-Fernandez and Ermentrout [10] for the vessel electrophysiology and vessel dimensions, and from Ursino et al. [33] for the elastic and muscle stress curves.

The phase plane of n versus v is given in Figure 3.5. The dashed curves are the nullclines for v and n . They intersect at a steady state that is unstable. The steady state is surrounded by a stable limit cycle, that is, an oscillation of both v and n . The corresponding solutions for v , Ca_i , ω , and r as functions of time are shown in Figure 3.6.

Parameter	Units	Value
A	cm^2	1.5×10^{-3}
τ	dyne s cm^{-2}	π
σ_{e0}		1.72×10^{-6}
k_e		21.63
r_0		0.56
S	cm^2	9.0×10^{-3}
L	cm	1
σ_0	dyne cm^{-2}	3.0×10^6
k_c		16.0
r_c		1
v_1	mV	-22.5
v_2	mV	25.0
v_3	mV	-15.0
v_4	mV	14.5
ϕ_n	s^{-1}	2.664
C	C mV^{-1}	1.9635×10^{-14}
g_l	$\text{C s}^{-1} \text{mV}^{-1}$	7.854×10^{-14}
g_k	$\text{C s}^{-1} \text{mV}^{-1}$	3.1416×10^{-13}
g_{Ca}	$\text{C s}^{-1} \text{mV}^{-1}$	1.57×10^{-13}
v_l	mV	-70.0
v_k	mV	-90.0
v_{Ca}	mV	80.0
α	nM C^{-1}	7.9976×10^{15}
K_d	nM	1.0×10^3
B_T	nM	1.0×10^5
Ca_{im}	nM	3.5×10^2
q		3
ψ_m		3.0×10^{-1}
k_ψ	s^{-1}	3.3
Δp	mmHg	100
r_{ref}	cm	3.128×10^{-2}

Table 3.1: Model parameters and their default values.

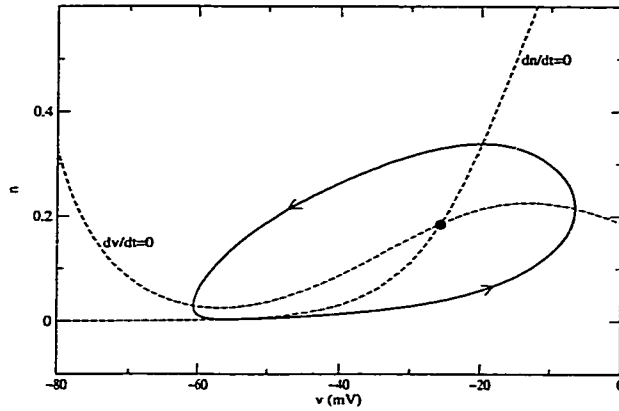


Figure 3.5: The phase plane of n versus v of the vasomotion model with parameters from Table 3.1. The dotted curves represent the nullclines for the v and n variables. The intersection of the nullclines is an unstable steady state. The solid curve represents the oscillating solution for v and n .

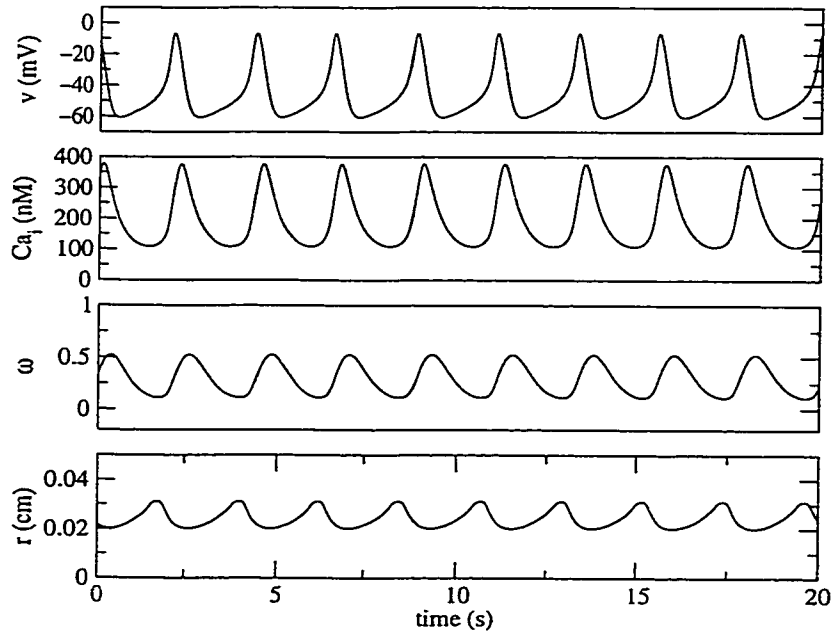


Figure 3.6: Solution of the vasomotion model for v , Ca_i , ω , and r as a function of time for the parameters given in Table 3.1.

3.4 Discussion

The parameters of the system are chosen such that an oscillation occurs in the v and n variables. This oscillation is carried through by Ca_i , ω , and finally r (vasomotion). Although the model is based on simple electrophysiology, it is sufficient for oscillating solutions that cause vasomotion.

The model is not complete as it does not directly take into account other factors that can affect vascular smooth muscle activity. For example, nitric oxide (NO) affects the open probability of the potassium channels, which affects the dynamics of the membrane potential, and ultimately the dynamics of the vessel radius. It will be shown in Chapter 4 that a simple change in one parameter can abolish cyclic activity and result in a static vessel. It is likely that such a parameter is in fact influenced by external factors that can place the vessel in an 'oscillatory domain' and a 'resting state domain.'

The next chapter looks into conditions under which the model, placed in the resting state domain, can account for characteristics of the myogenic response and the maintenance of myogenic tone.

Chapter 4

The myogenic response and the regulation of myogenic tone

The myogenic response is the ability of vascular smooth muscle to relax and contract in response to a change in blood pressure to regulate local blood flow [1]. Figure 4.1 illustrates the myogenic response observed in the skeletal muscle vascular bed of the dog. From a control pressure of 100 mmHg, the pressure was abruptly changed and the corresponding flow was immediately measured (solid circles). The flow was measured again under steady-state conditions, achieved after 30-60 seconds (open circles) [1]. In this example, the smooth muscle cells are successful at relaxing or contracting to maintain a constant flow rate for pressures ranging between 20 and 130 mmHg. At higher pressures, the smooth muscle cells are not as successful, but are successful at reducing the flow significantly.

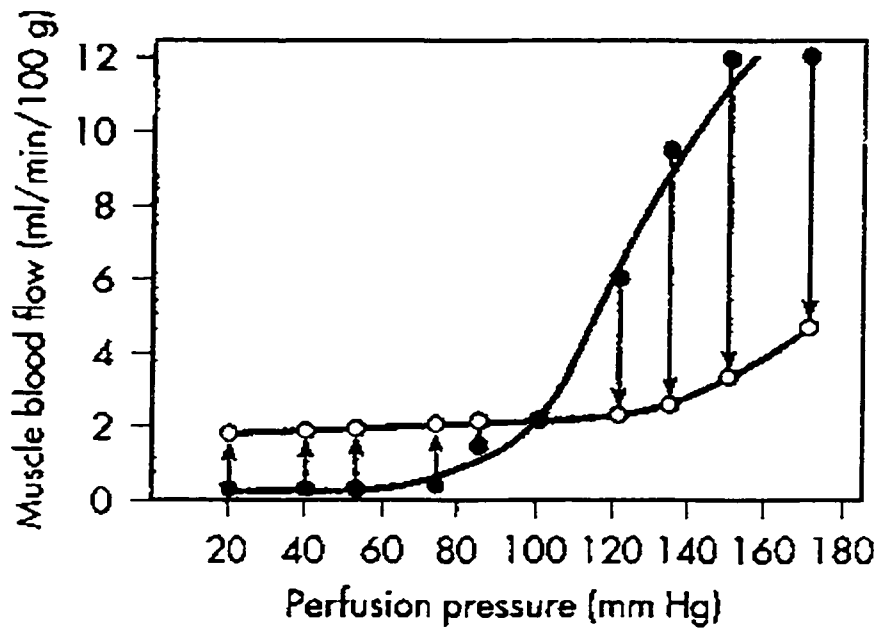


Figure 4.1: Pressure-flow relationship in the skeletal muscle vascular bed of the dog. Closed circles represent the muscle blood flow obtained immediately after abrupt changes in perfusion pressure from the control level of 100 mmHg. Open circles represent the steady-state flow obtained at the new perfusion pressure [1]. Plot taken from Berne and Levy [1], redrawn from Jones et al. [18]

The myogenic response and vasomotion are both a result of smooth muscle activity, which makes it a reasonable hypothesis that they are related phenomena [7, 32, 33]. The model for vasomotion presented in Chapter 3 is based on simple physiology of vascular smooth muscle. If it is true that vasomotion and the myogenic response are related, then characteristics of the myogenic response should be present in the model. In this chapter, mechanisms believed to be responsible for the myogenic response are investigated in the context of the model.

The first requirement for the model to account for myogenic behaviour is that it must be able to predict a stable steady state. A steady-state solution with $v \approx -64$ mV is obtained by setting $v_1 = -16$, which is in agreement with the reference resting membrane potential used by Harder [14] in his experiments. The solution of the modified model is shown in Figure 4.2 (solid curves). The vasomotion solution from Figure 3.6 has been superimposed for comparison (dotted curves). The resting vessel has a membrane potential less than that of vasomotion, which results in a reduced intracellular calcium concentration, relaxed muscle and hence greater radius. Note that modifying the parameter v_1 is not the only way to obtain a steady-state solution, however it will be the only one considered here.

During the myogenic response, membrane depolarization and an increase of intracellular calcium is observed. It is the increase of intracellular calcium that is believed to be involved in the *initiation* of the myogenic response. Section 4.1 will focus on proposed mechanisms for the initiation of the myogenic

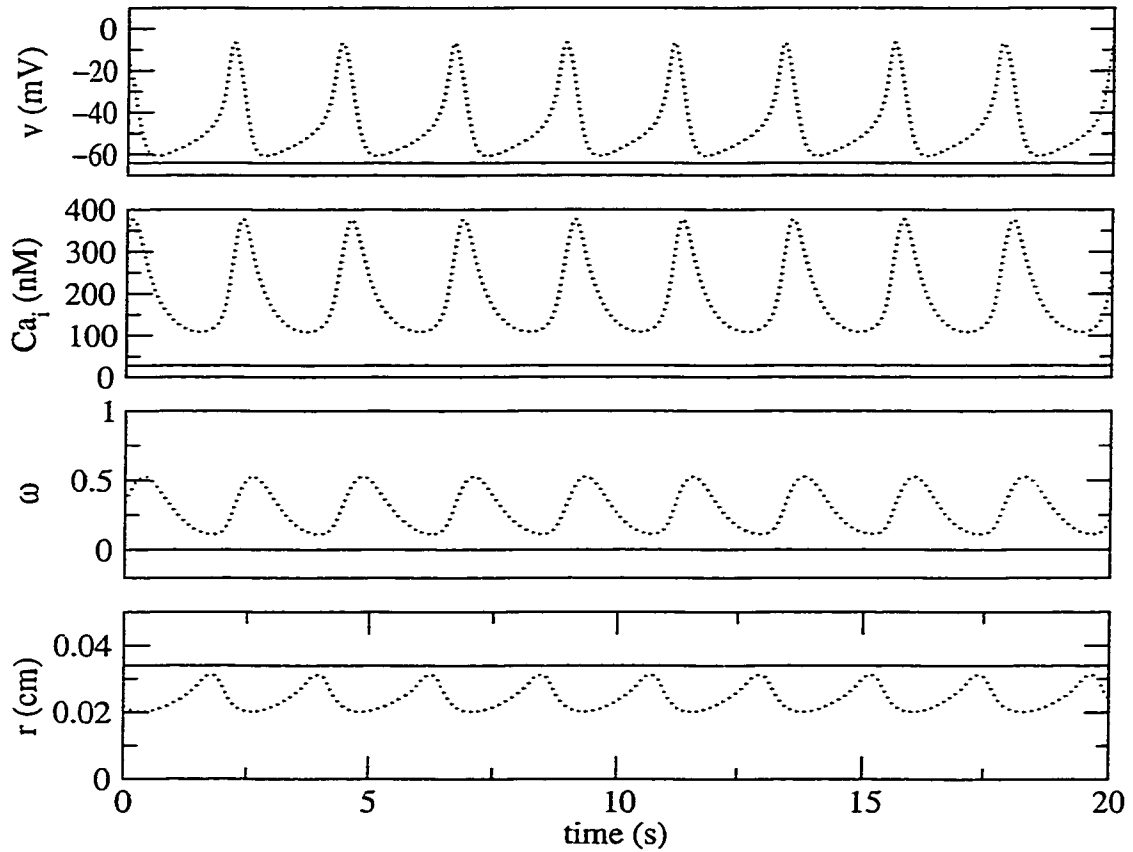


Figure 4.2: Steady-state solution (solid curves) for v , Ca_i , ω , and r . Parameter values are as listed in Table 3.1, except $v_1 = -16$. The vasomotion solution from Figure 3.6 has been superimposed for comparison (dotted curves).

response in the context of the model. However, after an initial transient, intracellular calcium concentration is observed to return to normal levels while stress production is maintained [4]. This observation has prompted investigation into the existence of alternate regulatory mechanisms that are responsible for the *maintenance* of myogenic tone [4]. In Section 4.2, a proposed mechanism for the maintenance of myogenic tone is discussed in the context of the model.

4.1 Initiation of the myogenic response

In this section, two theories on the cause of the initial increase in intracellular calcium concentration that is observed during the myogenic response are presented.

There is evidence of an ion channel that is sensitive to stretching of the cell membrane. These stretch-activated channels (SAC) are cation nonspecific, but contribute to the influx of ions which leads towards cell depolarization [4]. Depolarization increases the open probability of the voltage-dependent calcium channels, which in turn leads to an increase in intracellular calcium. In Section 4.1.1, currents due to stretch-activated channels are added to the model, and the qualitative behaviour of the modified model in response to stretch is demonstrated.

Even in the absence of extracellular calcium, an increase of intracellular calcium is observed in stretched vascular smooth muscle [4]. This observation

suggests the existence of an intracellular calcium store which can release calcium into the cytosol in response to stretch. In Section 4.1.2, the dynamics of an intracellular calcium store are added to the model, and the response of the modified model to an applied stretch is investigated.

4.1.1 Stretch-activated channels (SAC)

The existence of a stretch-activated ion channel may be sufficient to explain the initial depolarization of the membrane potential and the increase in intracellular calcium observed in stretched vascular smooth muscle cells. A depolarization of the membrane potential activates the voltage-dependent calcium channels which causes an increase in intracellular calcium, further depolarization, and the required stress production.

Kirber et al. [19] identified a cation nonspecific stretch-activated channel in the toad stomach permeable to Na^+ , K^+ , and Ca^{2+} , with unitary conductances of 58, 66, and 18.5 pS, respectively. It is the Na^+ current through this channel that is believed to initiate depolarization which in turn activates the voltage-dependent calcium channels [4].

The initial effect of a stretch-activated ion current on the steady state solution will be considered by introducing a current, I_s , to equation (3.13) to give

$$\frac{dv}{dt} = -[g_k n \cdot (v - v_k) + g_{Ca} m_\infty(v) \cdot (v - v_{Ca}) + g_l \cdot (v - v_l) + I_s] C^{-1}.$$

Since sodium is believed to be the ion which causes the initial depolarization, let $I_s = g_{Na}s \cdot (v - v_{Na})$, where g_{Na} , s , and v_{Na} , are the maximum whole-cell conductance of the sodium channels via the SAC, the fraction of open stretch-activated channels, and the sodium Nernst potential, respectively. The analysis will treat s as a parameter and the effect on the steady-state value of r will be analyzed. Ideally, the dynamics of s would be required, with a suitable dependence of s on r .

The analysis will assume a fast potassium channel to abolish oscillating activity by setting $\phi_n = 5$. In Figure 4.3, the nullclines of v and n with $s = 0$ are shown (solid curves). This situation corresponds to a stable steady-state at $v \approx -64$ mV. Increasing s to $s = 1$ causes the nullcline for v to deform and shift upwards (dotted curve). The new steady-state value of v is at approximately -28 mV. Without the fast potassium channel assumption, this steady-state would be the center of a stable limit cycle with small-amplitude oscillations. The fast potassium channel was assumed here to eliminate these oscillations.

With an increase of the membrane potential, v , the fraction of open calcium channels increases which causes an increase in intracellular calcium and a corresponding reduction of the radius, r . Figure 4.4 gives the steady-state dependence of the membrane potential, v , and the radius, r , on the parameter s . The figure shows that a reduction in radius can be accomplished by an increase of s . In reality, s would not be a parameter, but somehow dependent on stretch (changes in r from rest). It seems counterintuitive that this

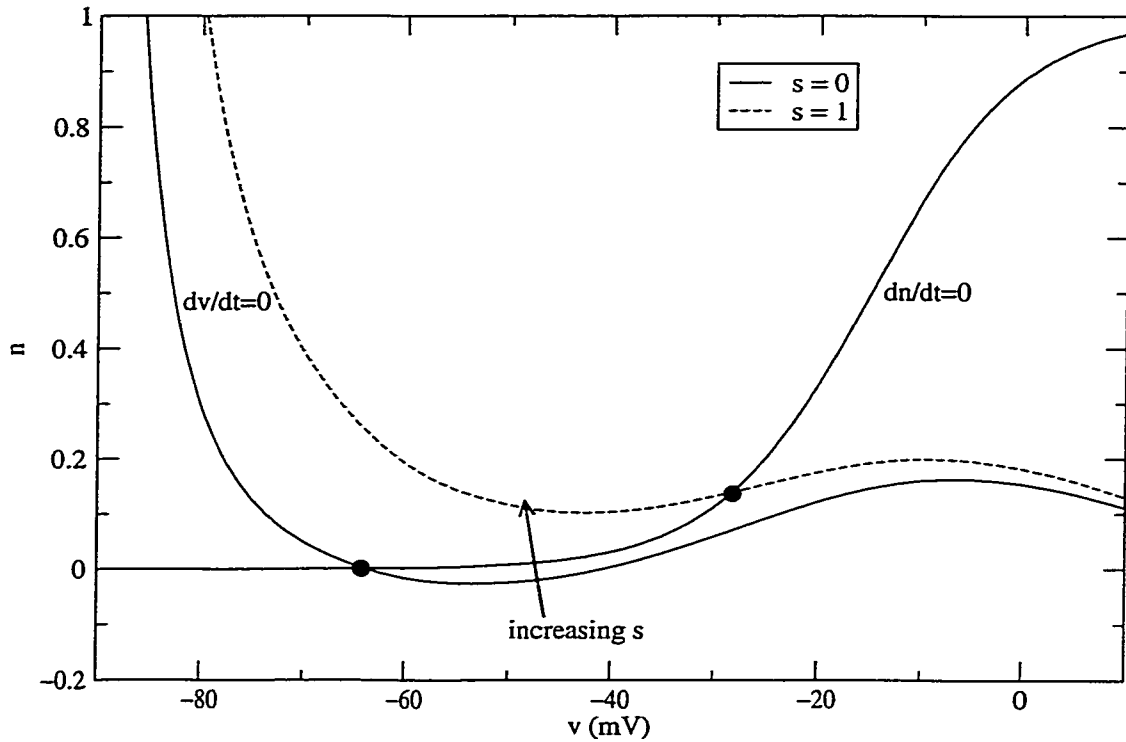


Figure 4.3: Nullclines $\frac{dn}{dt} = \frac{dv}{dt} = 0$, with $g_{Na} = 1$, $v_{Na} = 40$ mV, and $\phi_n = 5$. The intersection of the nullclines represents a stable steady state with $v \approx -64$ mV. When s is increased, the $\frac{dv}{dt} = 0$ nullcline moves in the direction of the arrow. The dotted nullcline shown is with $s = 1$. The applied current yields a new steady-state at $v \approx -28$ mV.

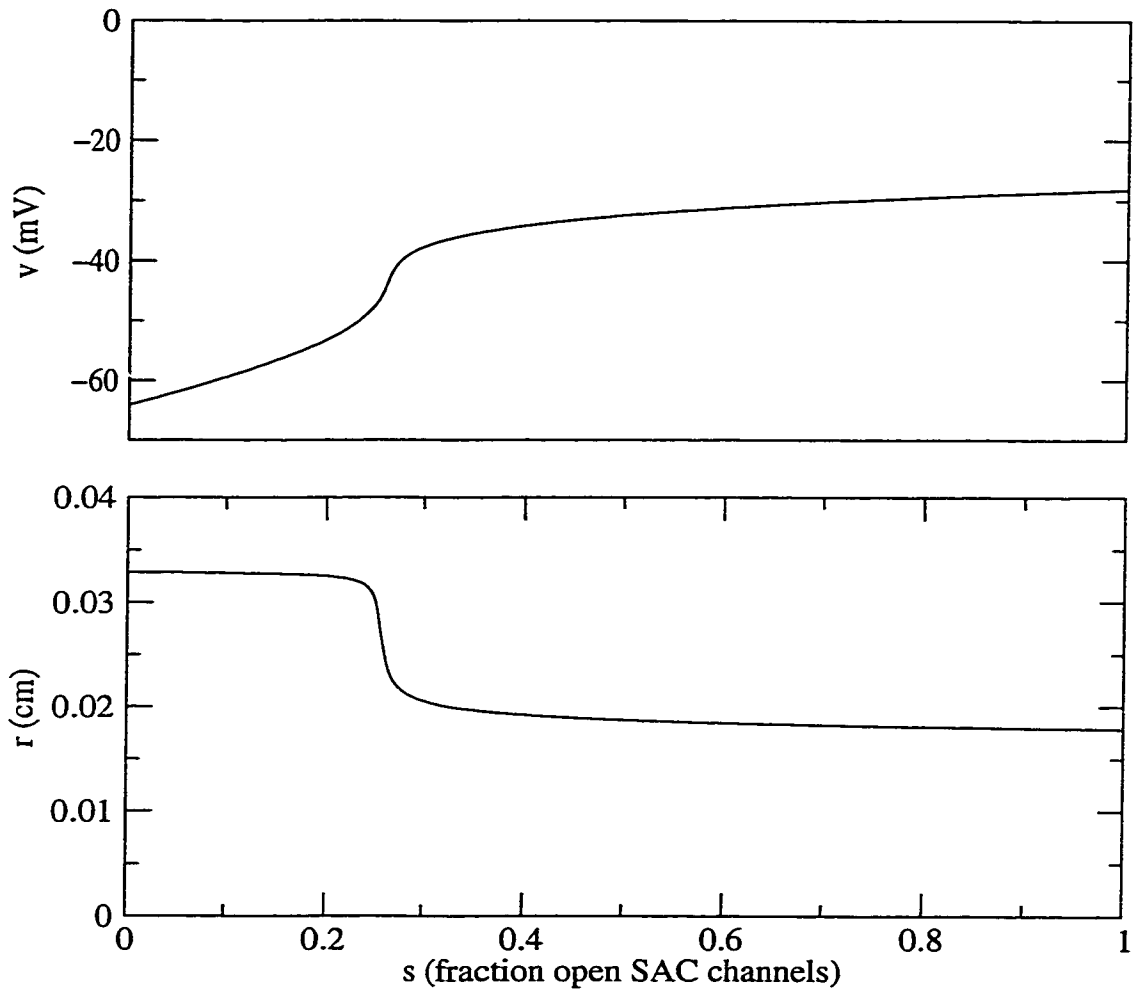


Figure 4.4: Steady-state dependence of the membrane potential, v , and vessel radius, r , on the fraction of open stretch-activated channels, s .

mechanism would work. Namely, if s increases in response to an increase in r , the eventual reduction of r due to s would abolish the stretch stimulus for s . The severity of this paradox depends on the dynamics of s on r . As shown in Figure 4.1, there is a 30-60 s delay in the activation of the myogenic response. This delay could be due to slowly activating stretch-activated channels. Similarly, a delay may also be present in the deactivation of s in response to changes in r , such that the removal of the stretch stimulus does not have an immediate effect on s . On the other hand, the stretch-activated channels may only have a short-lived effect on the intracellular calcium concentration, before another mechanism, such as the one discussed in Section 4.1.2, dominate.

4.1.2 Intracellular calcium stores and IP_3

A rise in intracellular calcium concentration in stretched vascular smooth muscle has been observed in the absence of extracellular calcium [4]. This observation suggests the involvement of an intracellular store for calcium ions. The *sarcoplasmic reticulum* (SR) is an intracellular organ with storage of calcium ions as its primary function. The SR takes in calcium via an ATP pump and releases calcium in response to 1,4,5-triphosphate (IP_3) stimulation [1].

Kulik et al. [20] studied the effect of stretching vascular smooth muscle cells on the concentration of intracellular IP_3 . They determined that with a stretch of 20% from rest, IP_3 was increased after 25 s but returned to control

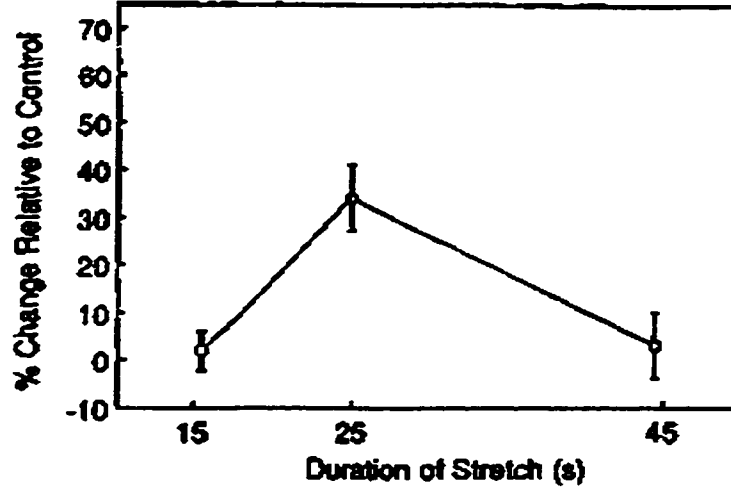


Figure 4.5: Experimental record of the relative change in intracellular IP_3 concentration of vascular smooth muscle after a single 20% stretch. Plot taken from Kulik et al. [20]

levels after 45 s [20], as shown in Figure 4.5. Since IP_3 stimulates the release of calcium from the SR [1], it is likely that this contributes to the initial increase of intracellular calcium observed during the myogenic response.

In order to investigate the role of the SR in the context of the model, equation (3.15) for the intracellular calcium concentration is modified by adding a term that describes the flux of calcium across the membrane of the SR. An equation describing the dynamics of the calcium concentration in the SR, Ca_{sr} , is introduced as well. The new calcium-handling equations are based on those found in Bertram et al. [2], and are as follows:

$$\begin{aligned} \frac{dCa_i}{dt} = & \frac{1}{\lambda} \left[\left(\frac{P_{leak}}{P_{ip3}} + O_{\infty} \right) (Ca_{sr} - Ca_i) - \frac{J_{er,p}}{P_{ip3}} \right] \\ & + [-\alpha I_{Ca} - k_{Ca} Ca_i] \rho, \end{aligned} \quad (4.1)$$

$$\frac{dCa_{sr}}{dt} = -\frac{1}{\sigma\lambda} \left[\left(\frac{P_{leak}}{P_{ip3}} + O_{\infty} \right) (Ca_{sr} - Ca_i) - \frac{J_{er,p}}{P_{ip3}} \right], \quad (4.2)$$

with

$$\begin{aligned} O_{\infty} &= a_{\infty} b_{\infty} h_{\infty}, \\ \frac{J_{er,p}}{P_{ip3}} &= v_{er,p} \frac{Ca_i^2}{Ca_i^2 + 90^2}, \\ a_{\infty} &= \frac{Ca_i}{Ca_i + 100}, \\ b_{\infty} &= \frac{IP_3}{IP_3 + 200}, \\ h_{\infty} &= \frac{400}{Ca_i + 400}, \end{aligned}$$

and $\frac{P_{leak}}{P_{ip3}}$, λ , σ , $v_{er,p}$, and IP_3 are parameters. Default values of these parameters are listed in Table 4.1. The second term of equation (4.1) is familiar as it is the same as in equation (3.15), and models the calcium flux through the cell membrane. The first term of equation (4.1) and equation (4.2) models the transport of calcium ions between the cytosol and the SR. In particular, the $\frac{P_{leak}}{P_{ip3}} (Ca_{sr} - Ca_i)$ term models the leak transport rate of calcium ions from the SR to the cytosol, and the $O_{\infty} (Ca_{sr} - Ca_i)$ term models the transport rate of calcium ions from the SR to the cytosol which depends on the intracellular calcium concentration, Ca_i , and the IP_3 concentration. The dependence of O_{∞} on Ca_i is via the a_{∞} and the h_{∞} terms. The a_{∞} term models activation in response to an increase of Ca_i , and the h_{∞} term models deactivation with excessive amounts of Ca_i . The dependence on the IP_3

Parameter	Units	Value
λ	s	0.25
σ		5
$v_{er,p}$	nM	240
$\frac{P_{leak}}{P_{ip3}}$		0.02
k_{Ca}	s^{-1}	70
ρ		0.01

Table 4.1: Parameters used in the modified model that incorporates the intracellular calcium stores.

concentration is sigmoidal, and increases with an increase in IP_3 . Finally, the $\frac{J_{er,p}}{P_{ip3}}$ term models the take-up of calcium back into the SR via the ATP pumps, with a sigmoidal rate dependence on Ca_i .

The effect of releasing calcium from the SR to the cytosol in response to IP_3 on the vessel radius is considered. In this model, changes in intracellular calcium have no effect on the membrane potential. Although there is evidence of ion channels that are sensitive to the intracellular calcium concentration, they are neglected in the model. Therefore, assume a resting vessel with $\Delta p = 50$ mmHg and $v = -60$ mV. At time $t = 10$ s, Δp is raised to 200 mmHg. The increase in Δp causes a quick increase in the vessel radius, r , which can be seen in the fourth panel of Figure 4.6. At this time, IP_3 is assumed to begin increasing, reaching a maximum level at $t = 35$ s, and then returning to normal levels by $t = 55$ s, mimicking the observation made by Kulik et al. [20]. The form of the IP_3 -versus-time curve is motivated by Figure 4.5, and is assumed to be bell shaped, as shown in the top panel of Figure 4.6. The lower panels show the response of Ca_{sr} , Ca_i , and the radius

as functions of time.

Transport of calcium from the intracellular stores to the cytosol occurs as soon as IP_3 starts to increase, with a corresponding change in radius shortly after. Intracellular calcium increases for about 20 s before starting to decrease. The decrease is likely due to activation of the ATP pumps in the cell membrane. At about 45 s after the initial stretch, IP_3 returns to control levels [20], which ceases the transport of calcium from the SR to the cytosol. At that point, intracellular calcium is returned to control levels, muscle contraction ceases, and the radius increases. Although it is barely noticeable in the figure, the calcium concentration in the SR slowly begins to increase back to control levels.

This modified model qualitatively shows that introducing the intracellular calcium stores that respond to increases in IP_3 by releasing calcium into the cytosol can account for the initial myogenic response seen in vascular smooth muscle. However, it does not demonstrate the maintenance of myogenic tone after calcium is returned to control levels, as seen at $t = 51$ s when the radius returns to resting levels. The maintenance of myogenic tone is believed to be due to a secondary mechanism, dealt with in the next section.

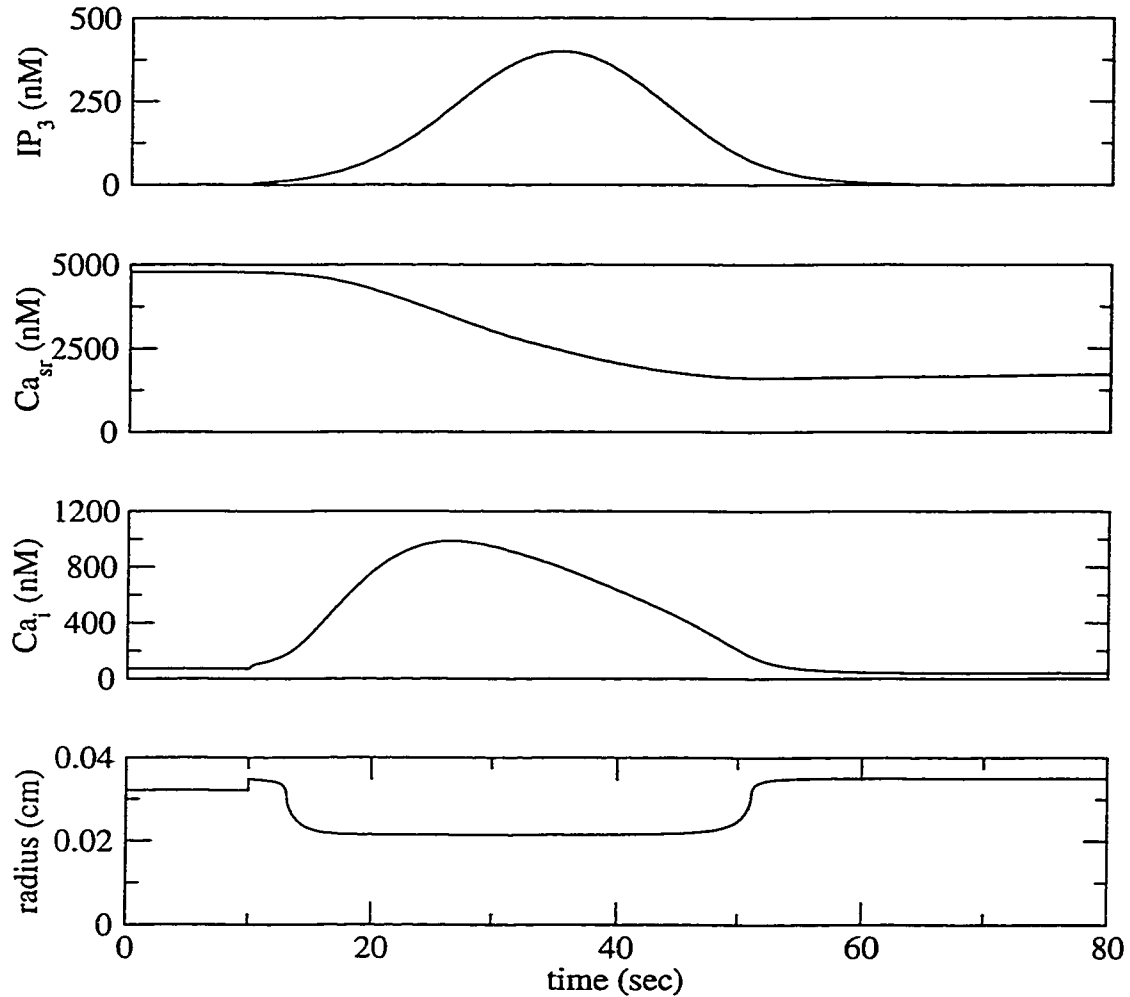


Figure 4.6: Solution of the vasomotion model modified to account for IP_3 -induced release of calcium from the intracellular stores. The system assumes that v is held constant at $v = -60$ mV. For the initial 10 s, $\Delta p = 50$ mmHg before being set to $\Delta p = 200$ mmHg for the remaining 70 s. Top panel: At $t = 10$ s, IP_3 is assumed to increase and peak at $t = 35$ s before tapering off at about $t = 55$ s. Bottom three panels: Response of calcium concentration in the SR, intracellular calcium, and radius.

4.2 A mechanism for the maintenance of myogenic tone

After the initial myogenic response, it is observed that the calcium concentration returns to control levels while stress production is maintained. This observation suggests the existence of a secondary mechanism responsible for maintaining the myogenic tone, different from those discussed in Section 4.1. In this section, a secondary mechanism which may be involved in the regulation of myogenic tone is examined.

Intracellular Protein Kinase C (PKC) has been shown to sensitize the contractile apparatus to intracellular calcium, such that a lower calcium concentration is required for stress production [30]. Furthermore, there is indirect evidence that suggests PKC is tonically active in pressurized arteries that exhibit myogenic tone [25], which suggests its role in the maintenance of myogenic tone.

The modulation of the sensitivity of muscle stress production on intracellular calcium concentration can be modeled by varying the Ca_{im} parameter in equation (3.21). Varying this parameter effectively alters the sensitivity of phosphorylation to the intracellular calcium concentration. In particular, decreasing Ca_{im} causes a left shift in ψ , and results in the ability to maintain muscle activation at lower intracellular calcium concentration levels than before. An assumption for the analysis that follows is that the intracellular calcium concentration is steady at $Ca_i = 100$ nM, which is consistent with

that of resting vascular smooth muscle [29]. The steady-state muscle activation, ω , and radius, r , as a function of Ca_{im} is shown in Figure 4.7, for various values of Δp . The figure shows that decreasing the parameter Ca_{im} (increasing the sensitivity) increases the muscle activation, ω , and hence decreases the radius, r .

For example, suppose a vessel is at rest with $\Delta p = 50$ mmHg and the calcium sensitivity, $\text{Ca}_{im} = 350$ (default value). Under these conditions, the vessel will have a radius of approximately $r = 0.026$ cm (solid curve). An increase of pressure to $\Delta p = 200$ will increase the radius to approximately $r = 0.034$ cm (dotted curve), well above the resting radius. The initial myogenic response will decrease the vessel radius (as discussed in Section 4.1), but will not be able to maintain the new radius for very long. Stress production can be maintained by decreasing the Ca_{im} parameter such that less calcium is required for stress production. For this example, letting $\text{Ca}_{im} = 150$ brings the system with $\Delta p = 200$ mmHg to a radius of approximately $r = 0.024$ cm.

4.3 Discussion

In this chapter, modifications to the vasomotion model presented in Chapter 3 were discussed in order to account for the myogenic response. In particular, two mechanisms for the initiation of the myogenic response and another for the maintenance of myogenic tone were presented.

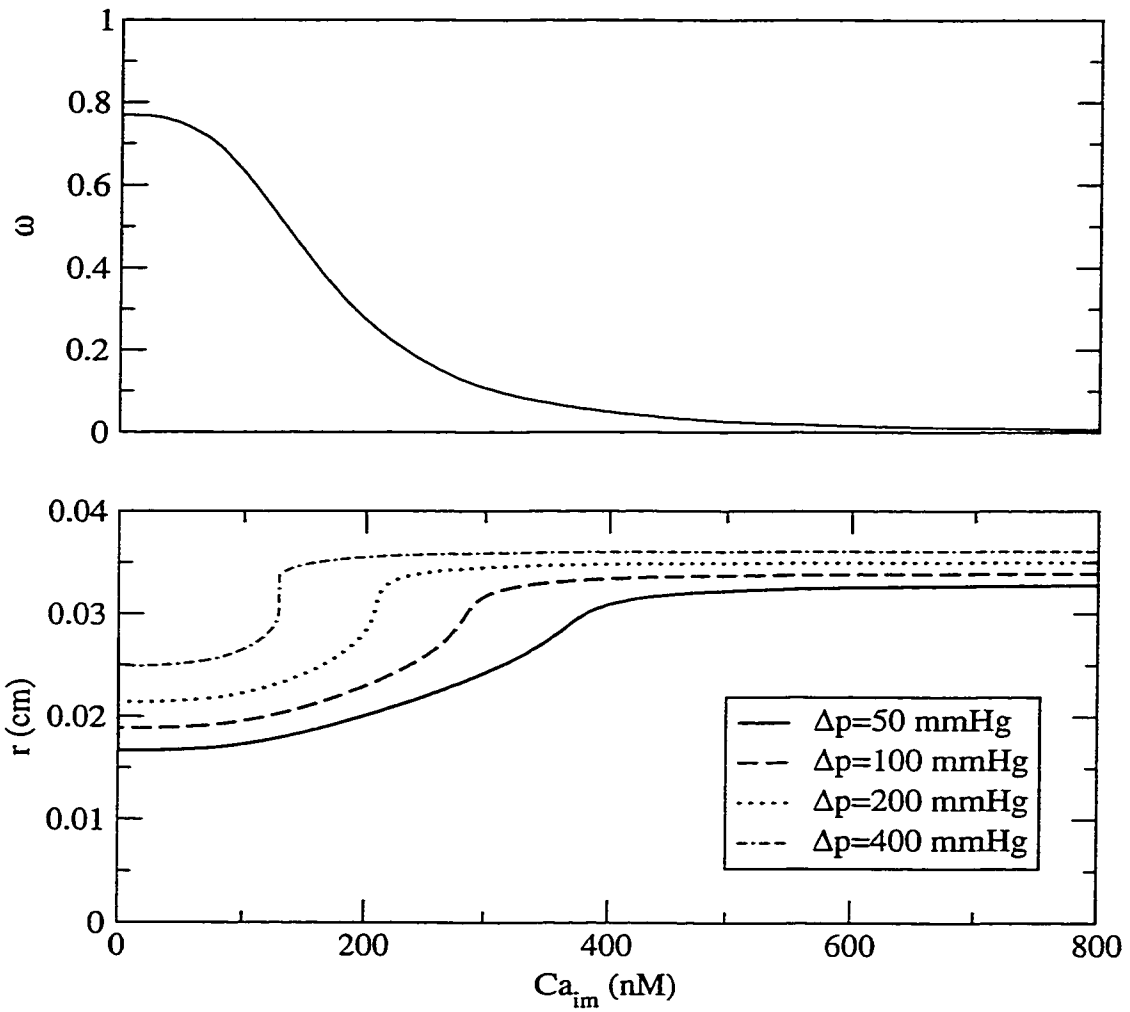


Figure 4.7: Steady-state dependence of muscle activation, ω , and radius, r , on the calcium concentration sensitivity parameter, Ca_{im} , for various transmembrane pressures, Δp . The intracellular calcium concentration is held fixed at $Ca_i = 100$ nM.

There is at least one additional hypothesis for the maintenance of myogenic tone. This hypothesis is based on a careful accounting of the various states of the myosin molecules involved in muscle stress production. In the model discussed in this thesis, three states for myosin are assumed: 1) unphosphorylated and unattached to actin, 2) phosphorylated and unattached to actin, and 3) phosphorylated and attached to actin. The “latch state” is a hypothesized fourth state for myosin that is unphosphorylated, still attached to actin, and producing stress [13]. Hai and Murphy [13] developed a kinetic model that essentially predicts the same fraction of attached crossbridges, ω , for a reduced intracellular calcium concentration, Ca_i , and a reduced fraction of phosphorylated crossbridges, ψ . The latch state model could be incorporated into the vasomotion model of Chapter 3. However, the same effect of the latch state model can be accomplished by varying the Ca_{im} (as was done in this chapter) and ψ_m parameters from equations (3.16) and (3.21), respectively. The advantage of the Hai and Murphy [13] model is that the transient solutions for changes in the intracellular calcium concentration qualitatively agree with experimental data. In conclusion, the latch state hypothesis can be modeled by varying the two parameters in the existing model, but it might be more interesting to consider the dynamical model of Hai and Murphy [13].

Chapter 5

Discussion and conclusions

In this thesis, some phenomena observed in resistance-sized vessels that are due to the action of vascular smooth muscle cells surrounding the vessel were examined. The myogenic response is the ability of vascular smooth muscle to contract or relax in order to regulate local blood flow in response to changes in blood pressure. Blood vessels are also observed to exhibit vasomotion, which is the spontaneous oscillation of the vessel radius. The purpose of vasomotion is not clear, but it is known to have an effect on vascular resistance and blood flow. It has also been hypothesized to be related to the myogenic response.

In Chapter 2, a model for the effect of vasomotion on blood flow and vascular resistance was analyzed. There is controversy in the published literature about the effect of vasomotion is analyzed on vascular resistance. Funk et al. [8] used a mathematical model to conclude that vascular resistance decreases with an increase in vasomotion amplitude, while Gratton et al. [11]

concluded the opposite. In this thesis, the modeling was reviewed and it was concluded that vasomotion alone decreases vascular resistance, in agreement with the modeling work of Funk et al. [8]. The disagreement with the modeling of Gratton et al. [11] stems from a misinterpretation of the definition of vascular resistance. The definition of vascular resistance only applies to steady-state flows or the steady-state component of flow. It is therefore not valid to consider a time-dependent vascular resistance or the time-average of it. “Time-dependent resistance” is actually the study of impedance theory (see Nichols et al. [24]).

In the model of Funk et al. [8], the radius in Poiseuille’s law is assumed to vary with time to give the instantaneous fluid volume flux at any moment. There is a potential problem with this assumption in that Poiseuille’s law is only applicable to steady-state flows, and flow is not at a steady state during vasomotion. However, conditions were derived in Chapter 2 under which the use of Poiseuille’s law in approximating vascular resistance during vasomotion is legitimate.

Another potential problem with the model is the non-Newtonian property of blood. This means that μ in Poiseuille’s law is not constant, but dependent on the flow characteristics. Blood plasma alone behaves like a Newtonian fluid, but it is the suspension of red blood cells which makes it non-Newtonian [24]. For steady flow, μ is understood to be the effective viscosity of the blood, and it depends on the fluid velocity, the vessel radius, and the red blood cell concentration. The problem arises when the vessel

radius is varied. This alters the effective viscosity of the blood, which in turn alters the fluid volume flux and the effective vascular resistance. For small oscillations of vessels with a mean radius of 200-350 μm , the effective viscosity does not change significantly [24] and can be considered constant (as was done throughout this thesis). However, for capillary-size vessels, a small change in the radius can have significant effects on the effective viscosity, and more care must be taken with any analysis.

The analysis in this thesis only considered the local effect of vasomotion on blood flow and vascular resistance. In reality, a blood vessel is a member of a large network of vessels that are in series and parallel. If each vessel were to be static, then the system can be modeled like a basic DC circuit and the flow characteristics over any segment can be predicted. Vasomotion in a vessel changes the dynamics of the network and causes fluctuations in pressure which alters blood flow characteristics in other parts of the network. It would be an interesting study to consider some basic networks of vessels, and the effect of vasomotion in one or some of the vessels, in and out of phase.

In Chapter 3, a model for vasomotion based on the model of Gonzalez-Fernandez and Ermentrout [10] was reviewed. The electrophysiology of the muscle cells is modeled by the Morris-Lecar [23] model, which models the transport of calcium and potassium ions through the cell membrane, the membrane potential, and the resulting intracellular calcium concentration. Since intracellular calcium is the primary stimulus for muscle contraction,

the calcium concentration is used to model the muscle activation, which is combined with the mechanics of the vessel in order to determine the vessel radius. The parameters of the model are such that an oscillation occurs in the membrane potential, which causes oscillations throughout the system, including that of the radius. This oscillation represents vasomotion.

In Chapter 4, modifications were made to the vasomotion model to investigate the validity of the theories on the mechanisms underlying the myogenic response. In particular, two theories were investigated for the *initiation* of the myogenic response, and one for the *maintenance* of myogenic tone. The first theory for initiation is the existence of stretch-activated channels in the membrane that causes membrane depolarization in response to cell deformation. Cell depolarization increases the flux of calcium into the cell and hence muscle contraction. The second theory is that of an intracellular calcium store that releases calcium into the cytosol in response to IP_3 stimulation. Finally, a theory on the maintenance of myogenic tone was discussed and an analysis on the sensitivity of the muscle contractile apparatus on the intracellular calcium concentration was performed. The results of the chapter give evidence that the vasomotion model can be extended to account for the myogenic response. The analysis presented is qualitative, but invites further research into the mathematics that describe smooth muscle physiology.

Since vascular smooth muscle activity regulates blood flow, it suggests the existence of a control mechanism for vascular smooth muscle activity. It is this control system that regulates the amount of muscle contraction such

that the proper radius is achieved to bring blood flow back to control levels. However, it is not exactly clear how this control mechanism works. A vessel experiences a normal stress from the transmural pressure (as discussed in Chapter 4) and a shear stress from the intraluminal pressure gradient. It is likely that these stresses regulate the myogenic response by causing the release of chemical messengers that subsequently stimulate the contractile apparatus of vascular smooth muscle. Some experiments have shown that an intact endothelium (the cellular lining of the inner vessel wall) is required for the myogenic response [14]. Furthermore, it has been shown that the endothelium can release nitric oxide (a vasodilator) in response to shear stress, and endothelin (a powerful vasoconstrictor) [1]. These observations suggest a role for the endothelium in the control mechanism of smooth muscle activity, and motivate future extensions of the model.

The analysis of the model has primarily dealt with the electrophysiology that controls the intracellular calcium concentration. Future investigation of the model may consider questions such as variations in the mechanical properties of blood vessels. These properties may include the observed stiffening of blood vessels that occurs with aging. An initial analysis of this phenomenon would include changes in the elastic properties of the vessel, by altering the properties of the elastic component of the free body diagram shown in Figure 3.2. As the model stands, a smaller steady-state radius would be predicted as a result of an increased vessel stiffness. However, this change in radius would alter the blood flow characteristics which could alter the control

mechanism for smooth muscle activity. This example highlights the importance of extending the model to account for the control system of vascular smooth muscle by the blood flow.

In conclusion, the model reviewed in Chapter 3 can account for some of the phenomena observed in blood vessels. It stands as a good foundation for extensions to account for the myogenic response, and possibly other mechanisms that control vascular smooth muscle activity.

Bibliography

- [1] R. M. BERNE AND M. N. LEVY, *Cardiovascular Physiology*, Mosby-Year Book, Inc., 7 ed., 1997.
- [2] R. BERTRAM, P. SMOLEN, A. SHERMAN, D. MEARS, I. ATWATER, F. MARTIN, AND B. SORIA, *A role for calcium release-activated current (CRAC) in cholinergic modulation of electrical activity in pancreatic β -cells*, *Biophys. J.*, 68 (1995), pp. 2323–2332.
- [3] R. S. BRODKEY, *The Phenomena of Fluid Motions*, Addison-Wesley Series in Chemical Engineering, Addison-Wesley Pub. Co., 1967.
- [4] G. D'ANGELO AND G. A. MEININGER, *Transduction mechanisms involved in the regulation of myogenic activity*, *Hypertension*, 23 (1994), pp. 1096–1105.
- [5] A. B. EBEIGBE AND M. EZIMOKHAI, *Vascular smooth muscle responses in pregnancy induced hypertension*, *Trends Pharmacol. Sci.*, 9 (1988), pp. 455–457.

- [6] G. B. ERMENTROUT. XPP -
<http://www.cnbc.cmu.edu/people/ermentrout.html>.
- [7] B. FOLKOW, *Description of the myogenic hypothesis*, *Circ. Res.*, 14 and 15 (1964), pp. I279–I287.
- [8] W. FUNK, D. ENDRICH, K. MESSMER, AND M. INTAGLIETTA, *Spontaneous arteriolar vasomotion as a determinant of peripheral vascular resistance*, *Int. J. Micro. Circ. Clin.*, 2 (1983), pp. 11–25.
- [9] J. M. GONZALEZ-FERNANDEZ, 1999. Personal correspondence.
- [10] J. M. GONZALEZ-FERNANDEZ AND B. ERMENTROUT, *On the origin and dynamics of the vasomotion of small arteries*, *Math. Biosci.*, 119 (1994), pp. 127–167.
- [11] R. J. GRATTON, R. E. GANDLEY, J. F. MCCARTHY, W. K. MICHALUK, B. K. SLINKER, AND M. K. MCLAUGHLIN, *Contribution of vasomotion to vascular resistance: a comparison of arteries from virgin and pregnant rats*, *J. Appl. Physiol.*, 85 (1998), pp. 2255–2260.
- [12] H. GUSTAFSSON, *Vasomotion and underlying mechanisms in small arteries*, *Acta. Physiol. Scand.*, 149 (1993), pp. 1–44.
- [13] C.-M. HAI AND R. A. MURPHY, *Cross-bridge phosphorylation and regulation of latch state in smooth muscle*, *Am. J. Physiol.*, 254 (1988), pp. C99–C106.

- [14] D. HARDER, *Pressure-induced myogenic activation of cat cerebral arteries is dependent on intact endothelium*, *Circ. Res.*, 60 (1987), pp. 102–107.
- [15] A. L. HODGKIN AND A. F. HUXLEY, *A quantitative description of membrane current and its application to conduction and excitation in nerve*, *J. Physiol. (London)*, 117 (1952), pp. 500–544.
- [16] N. IIDA, *Physical properties of resistance vessel wall in peripheral blood flow regulation - I. mathematical model*, *J. Biomechanics*, 22 (1989), pp. 109–117.
- [17] M. INTAGLIETTA, *Arteriolar vasomotion: Implications for tissue ischemia*, *Blood Vessels*, 28 (1991), pp. 1–7.
- [18] R. JONES AND R. BERNE. *Circ. Res.*, 1964.
- [19] M. T. KIRBER, J. V. WALSH, AND J. J. SINGER, *Stretch-activated ion channels in smooth muscle: a mechanism for the initiation of stretch-induced contraction*, *Pflugers Arch.*, 412 (1988), pp. 339–345.
- [20] T. J. KULIK, R. A. BIALECKI, W. S. COLUCCI, A. ROTHMAN, E. T. GLENNON, AND R. H. UNDERWOOD, *Stretch increases inositol triphosphate and inositol tetrakisphosphate in cultured pulmonary vascular smooth muscle cells*, *Biochem. Biophys. Res. Commun.*, 180 (1991), pp. 982–987.

- [21] P. K. KUNDU, *Fluid Mechanics*, Academic Press Inc., San Diego, CA, 1990.
- [22] M. C. MEYER, J. E. BRAYDON, AND M. K. McLAUGHLIN, *Characteristics of vascular smooth muscle in maternal resistance circulation during pregnancy in the rat*, Am. J. Obstet. Gynecol., 169 (1993), pp. 1510–1516.
- [23] C. MORRIS AND H. LECAR, *Voltage oscillations in the barnacle giant muscle fiber*, Biophys. J., 35 (1981), pp. 193–213.
- [24] W. W. NICHOLS AND M. F. O’ROURKE, *McDonald’s Blood Flow in Arteries*, Oxford University Press Inc., New York, 4 ed., 1998.
- [25] G. OSOL, I. LAHER, AND M. KELLEY, *Myogenic tone is coupled to phospholipase C and G protein activation in small cerebral arteries*, Am. J. Physiol., 265 (1993), pp. H415–H420.
- [26] D. PARTHIMOS, D. H. EDWARDS, AND T. M. GRIFFITH, *Comparison of chaotic and sinusoidal vasomotion in the regulation of microvascular flow*, Cardiovasc. Res., 31 (1996), pp. 388–399.
- [27] A. R. PRIES, T. W. SECOMB, AND P. GAEHTGENS, *Structural adaptation and stability of microvascular networks: theory and simulations*, Am. J. Physiol., 275 (1998), pp. H349–H360.

- [28] C. M. REMBOLD AND R. A. MURPHY, *Latch-bridge model in smooth muscle: $[Ca^{2+}]_i$ can quantitatively predict stress*, Am. J. Physiol., 259 (1990), pp. C251–C257.
- [29] R. RHOADES AND R. PFLANZER, *Human Physiology*, Saunders College Publishing, 3 ed., 1996.
- [30] K. SATO, M. HORI, H. OZAKI, H. TAKANO-OHMURO, T. TSUCHIYA, H. SUGI, AND H. KARAKI, *Myosin phosphorylation-independent contraction induced by phorbol ester in vascular smooth muscle*, J. Pharmacol. Exp. Ther., 261 (1992).
- [31] D. W. SLAAF, H. H. E. OUDE VRIELINK, G.-J. TANGELDER, AND R. S. RENEMAN, *Effective diameter as a determinant of local vascular resistance in presence of vasomotion*, Am. J. Physiol., 255 (1988), pp. H1240–H1243.
- [32] N. STERGIOPULOS, C. A. PORRET, S. DE BROUWER, AND J. J. MEISTER, *Arterial vasomotion: effect of flow and evidence of nonlinear dynamics*, Am. J. Physiol., 274 (1998), pp. H1858–H1864.
- [33] M. URSINO AND G. FABBRI, *Role of the myogenic mechanism in the genesis of microvascular oscillations (vasomotion): analysis with a mathematical model*, Microvasc. Res., 43 (1992), pp. 156–177.